steeper; the gain was thus higher and the coherence was lower in $H_{\text{n-closed-spon}}$ compared with $H_{\text{n-open}}$. The phase led as frequency increased, while the step response oscillated (Fig. 4*F*, left panel) in $H_{\text{n-closed-spon}}$, which were markedly different from $H_{\text{n-open}}$.

In contrast to the neural arc, the closed-loop-spontaneous transfer function for the peripheral arc ($H_{\text{p-closed-spon}}$) from SNA to AP (Fig. 4*E*, right panels, black line) approximated that of the open-loop transfer function ($H_{\text{p-open}}$, red line). The gain (except at 0.02–0.05 Hz) and phase were similar up to 0.3 Hz, although the coherence was lower in $H_{\text{p-closed-spon}}$ than in $H_{\text{p-open}}$ (common feature for both neural and peripheral arcs). The step response was similar to that of $H_{\text{p-open}}$ except for a slower time constant (Fig. 4*F*, right panel). Because of the closed-loop condition, the gain and phase functions of $H_{\text{p-closed-spon}}$ were the inverse of those of $H_{\text{n-closed-spon}}$.

Since CSP exactly matched systemic AP in this closed-loop-spontaneous baroreflex condition, the transfer function of total arc baroreflex from CSP input to systemic AP was calculated as all-pass filter without modulating phase (Fig. 4*D*). This is greatly different from the transfer function of the total arc identified from open-loop experiments (Fig. 3*E*).

Comparison between open-loop and closed-loop-spontaneous transfer functions

The closed-loop-spontaneous transfer functions (Fig. 5*A*, blue lines) ($H_{\text{n-closed-spon}}$ and $H_{\text{p-closed-spon}}$) obtained from

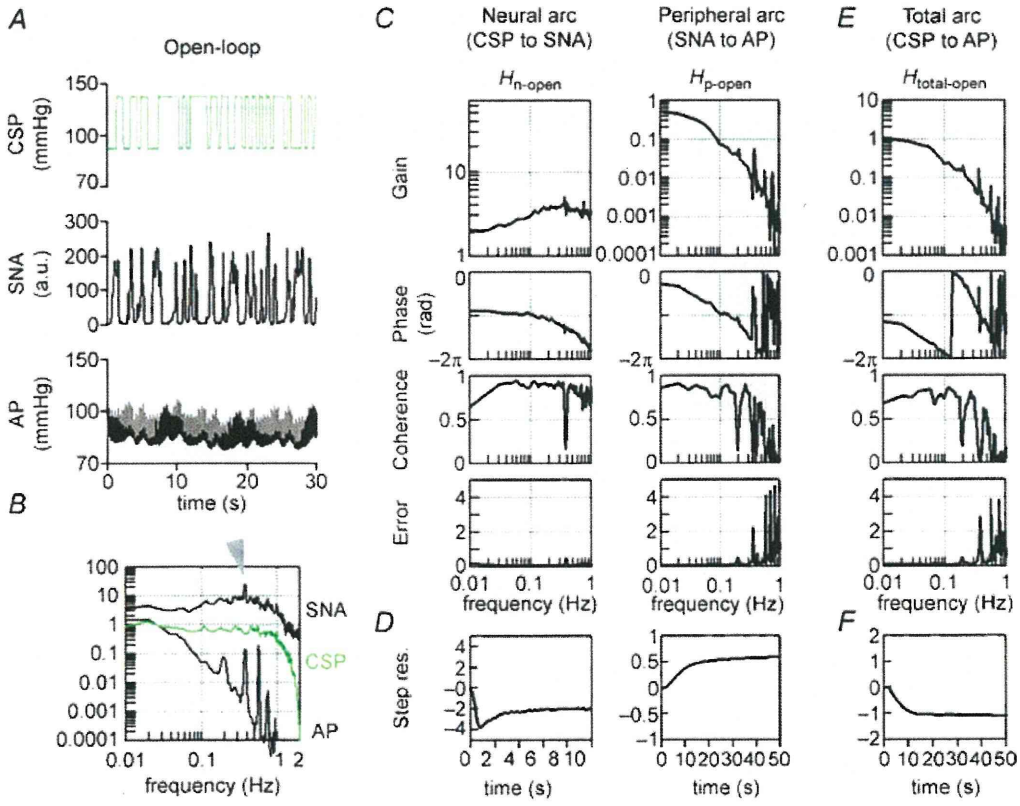

Figure 3. Open-loop transfer function
A, typical representative data of one rabbit in protocol 2, showing time series of carotid sinus pressure (CSP), sympathetic nerve activity (SNA) and systemic arterial pressure (AP) during CSP perturbation in open-loop baroreflex condition. CSP is changed according to a binary random (white-noise) signal with a switching interval of 500 ms. *B*, input power spectrum of CSP (green line) is reasonably flat up to 1 Hz. Autospectra of SNA (top line) and systemic AP (bottom line) are also shown. The arrowhead indicates a peak of SNA autospectrum at 0.4 Hz. *C*, open-loop transfer functions of the neural arc ($H_{\text{n-open}}$) from CSP input to SNA (left panels) and of the peripheral arc ($H_{\text{p-open}}$) from SNA input to AP (right panels) identified in the same animal as in A. The gain (top), phase (second), coherence (third) and normalized random error (Error, bottom) functions are shown. Units of gain are [a.u. mmHg^{-1}] for the neural arc and [mmHg a.u.^{-1}] for the peripheral arc, respectively. *D*, step responses (Step res.) derived from the transfer functions shown in *C*. The units are [a.u.] for the neural arc and [mmHg] for the peripheral arc, respectively. *E*, open-loop transfer functions of the total arc ($H_{\text{total-open}}$) from CSP input to AP identified in the same animal as in A. The gain (top), phase (second), coherence (third) and normalized random error (Error, bottom) functions are shown. Unit of gain is [mmHg mmHg^{-1}]. *F*, step response (Step res.) derived from the transfer function shown in *E*. The unit is [mmHg]. a.u., arbitrary unit.

all animals ($n = 10$) in protocol 2 were compared with the open-loop transfer functions (Fig. 5*A*, red lines) in protocol 1. The step response was also compared between closed-loop-spontaneous (Fig. 5*B*, blue line) and open-loop experiments (Fig. 5*B*, red line).

In the neural arc (Fig. 5*A* and *B*, left panels; Table 1), closed-loop-spontaneous transfer functions ($H_{\text{n-closed-spon}}$, blue lines) were markedly different from open-loop transfer functions ($H_{\text{n-open}}$, red lines), similar to the example shown in Fig. 4*E*. The difference was characterized by an enhanced increase of gain *versus* frequency (slope), a phase lead and an oscillation of step response. In contrast, in the peripheral arc (Fig. 5*A* and *B*, right panels; Table 2), closed-loop-spontaneous transfer functions ($H_{\text{p-closed-spon}}$) were similar to open-loop transfer functions ($H_{\text{n-open}}$) in gain, phase and step response.

The transfer function of the baroreflex total arc from CSP input to systemic AP in the open-loop condition was identified as having low-pass filter characteristics with negative feedback in all animals. In contrast, the total arc transfer function in the closed-loop-spontaneous condition had all-pass filter characteristics without modulating phase in all animals.

Predictability of open-loop and closed-loop-spontaneous transfer function compared with data measured in open-loop condition (protocol 3)

The ability of the neural arc transfer functions (determined by protocols 1 and 2) to predict output dynamics (SNA) from given input signals (CSP) in the open-loop

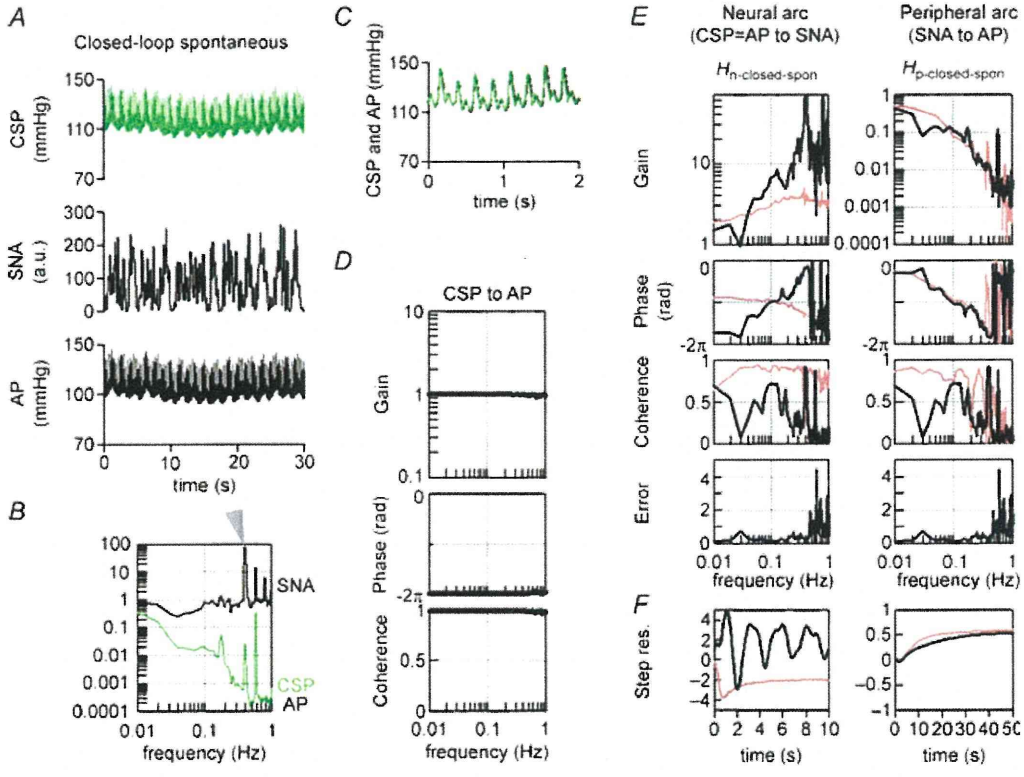

Figure 4. Closed-loop-spontaneous transfer function
A, typical representative data of protocol 3, showing time series of CSP, SNA and systemic AP in closed-loop-spontaneous baroreflex condition, where CSP is matched with systemic AP. The data were obtained from the same animal as in Figure 3. *B–D* show exactness of good match between CSP and systemic AP. *B*, autospectrum of CSP (green line) overlaps with that of AP (black line). Autospectrum of SNA (top line) is also shown. The arrowhead indicates a peak in the SNA autospectrum at 0.4 Hz. *C*, beat-to-beat waveform of CSP (green line) overlaps with that of AP (black line). *D*, the transfer functions from CSP to systemic AP. Gain (top), phase (middle) and coherence (bottom) functions are shown. Unit of gain is [mmHg mmHg^{-1}]. *E*, the closed-loop-spontaneous transfer functions of the neural arc ($H_{\text{n-closed-spon}}$) from CSP (=AP) input to SNA (left panels) and of the peripheral arc ($H_{\text{p-closed-spon}}$) from SNA input to AP (right panels) identified in the same animal as in *A*. The gain (top), phase (second), coherence (third) and normalized random error (bottom) functions are shown. Units of gain are [a.u. mmHg^{-1}] for the neural arc and [mmHg a.u.$^{-1}$] for the peripheral arc, respectively. *F*, step responses (Step res.) derived from the transfer functions. The units are [a.u.] for the neural arc and [mmHg] for the peripheral arc, respectively. a.u., arbitrary unit; CSP, carotid sinus pressure; SNA, sympathetic nerve activity; AP, arterial pressure; Step res., step response. In *E* and *F*, the open-loop transfer functions and derived step responses are included for reference (red lines).

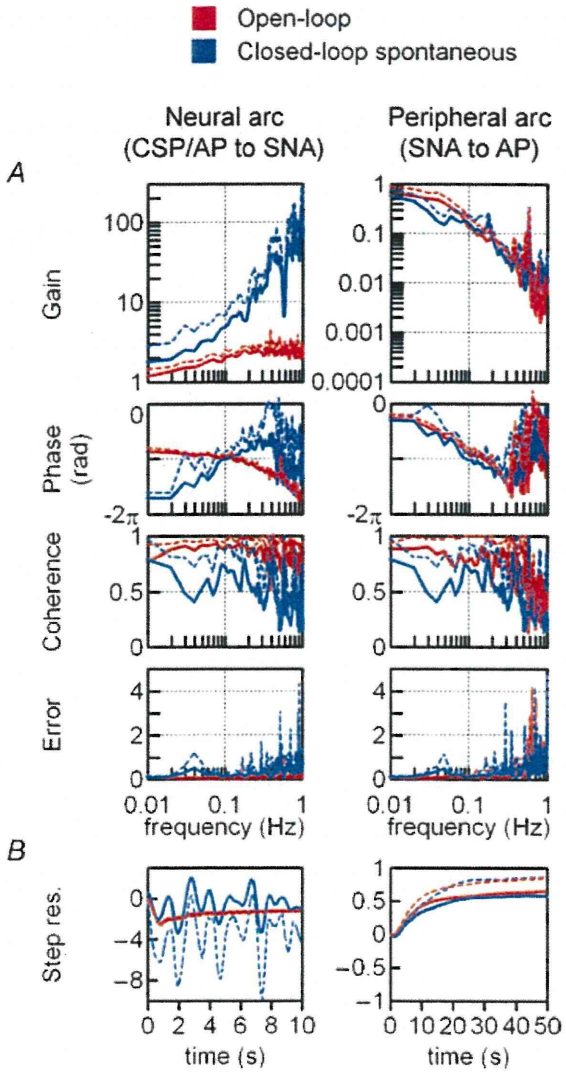

Figure 5. Comparison between open-loop and closed-loop-spontaneous transfer functions
Solid and dashed lines represent the mean and mean + SD, respectively, obtained from all animals (n = 10). *A*, red lines are open-loop transfer functions of the neural ($H_{n\text{-}open}$, left panels) and peripheral arcs ($H_{p\text{-}open}$, right panels) identified in protocol 1. Blue lines are closed-loop-spontaneous transfer functions (blue lines) of the neural ($H_{n\text{-}closed\text{-}spon}$, left panels) and peripheral arcs ($H_{p\text{-}closed\text{-}spon}$, right panels) identified in protocol 2. The gain (top), phase (second), coherence (third) and normalized random error (bottom) functions are shown. Units of gain are [a.u. $mmHg^{-1}$] for the neural arc and [mmHg $a.u.^{-1}$] for the peripheral arc, respectively. The closed-loop-spontaneous baroreflex transfer function for the neural arc is markedly different from the open-loop transfer function, whereas that for the peripheral arc partially matches the open-loop transfer function. *B*, step response (Step res.) calculated from the open-loop (red lines) and closed-loop-spontaneous (blue lines) transfer functions. The units are [a.u.] for the neural arc and [mmHg] for the peripheral arc, respectively. a.u., arbitrary unit; CSP, carotid sinus pressure; SNA, sympathetic nerve activity; AP, arterial pressure; Step res., step response.

Table 1. Transfer functions of the baroreflex neural arc (from CSP to SNA) in open-loop and closed-loop-spontaneous conditions

	Open-loop TF ($H_{n\text{-}open}$, CSP to SNA)	Closed-loop-spontaneous TF ($H_{n\text{-}closed\text{-}spon}$, CSP [= AP] to SNA)
Gain (a.u. $mmHg^{-1}$)		
0.01 Hz	1.2 ± 0.2	1.8 ± 0.1*
0.1 Hz	2.0 ± 0.3	5.3 ± 2.8*
0.3 Hz	2.6 ± 0.3	14.6 ± 5.7*
Phase (rad)		
0.01 Hz	−2.7 ± 0.2	−5.4 ± 0.4*
0.1 Hz	−3.0 ± 0.1	−3.1 ± 0.4
0.3 Hz	−3.7 ± 0.1	−2.6 ± 0.11*
Coherence		
0.01 Hz	0.8 ± 0.1	0.8 ± 0.2
0.1 Hz	0.9 ± 0.1	0.6 ± 0.2*
0.3 Hz	0.9 ± 0.1	0.4 ± 0.3*
Slope (dB per decade)		
0.01 Hz to 0.3 Hz	4.7 ± 0.4	12.1 ± 6.1*
Step response		
Initial response (a.u.)	−2.4 ± 0.2	Oscillating response
Steady-state level (a.u.)	−1.2 ± 0.2	

Values are mean ± SD ($n = 10$). *$P < 0.05$; open-loop *vs.* closed-loop-spontaneous conditions. TF, transfer function.

Table 2. Transfer functions of baroreflex peripheral arc (from SNA to AP) in open-loop and closed-loop-spontaneous conditions

	Open-loop TF ($H_{p\text{-}open}$, SNA to AP)	Closed-loop-spontaneous TF ($H_{p\text{-}closed\text{-}spon}$, SNA to AP)
Gain (mmHg $a.u.^{-1}$)		
0.01 Hz	0.7 ± 0.2	0.6 ± 0.2
0.1 Hz	0.1 ± 0.1	0.1 ± 0.1
0.3 Hz	0.03 ± 0.01	0.03 ± 0.02
Phase (rad)		
0.01 Hz	−0.8 ± 0.2	−0.9 ± 0.2
0.1 Hz	−3.0 ± 0.2	−3.0 ± 0.2
0.3 Hz	−4.2 ± 0.1	−4.0 ± 0.3
Coherence		
0.01 Hz	0.9 ± 0.1	0.8 ± 0.2
0.1 Hz	0.8 ± 0.2	0.6 ± 0.2*
0.3 Hz	0.9 ± 0.1	0.4 ± 0.3*
Step response		
Steady-state level (mmHg)	−0.7 ± 0.2	−0.6 ± 0.2

Values are mean ± SD ($n = 10$). *$P < 0.05$; open-loop *vs.* closed-loop-spontaneous conditions. TF, transfer function.

condition was quantified by comparing with the actual measurements of SNA response to CSP changes in protocol 3. Figure 6 shows a typical example obtained from the same animal as in Figs 1 and 2. CSP was randomly

Table 3. Predictive power of baroreflex transfer functions

	Open-loop TF ($H_{n\text{-}open}$, CSP to SNA)		Closed-loop-spontaneous TF ($H_{n\text{-}closed\text{-}spon}$, CSP [= AP] to SNA)	
	r^2	(Predicted condition)	r^2	(Predicted condition)
Neural arc	0.8 ± 0.1*	(Open-loop)	0.1 ± 0.1	(Open-loop)
	0.1 ± 0.2	(Closed-loop-spon)	0.06 ± 0.1	(Closed-loop-spon)
	0.9 ± 0.1*	(Closed-loop-drug)	0.7 ± 0.1(r < 0[a])	(Closed-loop-drug)
	Open-loop TF ($H_{p\text{-}open}$, SNA to AP)		Closed -loop-spontaneous TF ($H_{p\text{-}closed\text{-}spon}$, SNA to AP)	
	r^2	(Predicted condition)	r^2	(Predicted condition)
Peripheral arc	0.8 ± 0.1*	(Open-loop)	0.7 ± 0.1*	(Open-loop)
	0.7 ± 0.1*	(Closed-loop-spon)	0.7 ± 0.1*	(Closed-loop-spon)

Values are mean ± SD ($n = 10$). *$P < 0.05$; significant correlation between predicted and measured values. [a]Regarding the predictive power of closed-loop-spontaneous TF in neural arc closed-loop-drug condition, r is less than 0 ($r = -0.8 \pm 0.1$). TF, transfer function; Open-loop, baroreflex open-loop condition where CSP was binary random (white-noise) sequence and independent of systemic AP; Closed-loop-spon, baroreflex closed-loop-spontaneous condition where CSP equalled systemic AP; Closed-loop-drug, sequential infusions of phenylephrine and nitroprusside in closed-loop condition where CSP equalled systemic AP.

assigned at 20 mmHg above or below the operating AP (changes according to binary random (white-noise) sequence; Fig. 6*A*, top panel). The SNA response to CSP changes predicted by the open-loop transfer function ($H_{n\text{-}open}$) (Fig. 6*A*; third panel) resembled the actually measured SNA (Fig. 6*A*, second panel) in both the timing (phase) and magnitude of neural burst. In contrast, the SNA response predicted by the closed-loop-spontaneous transfer function ($H_{n\text{-}closed\text{-}spon}$) (Fig. 6*A*, bottom panel) was different from the actually measured SNA (Fig. 6*A*, second panel), showing markedly exaggerated fluctuation and inconsistent burst timing. As a result, scatter plot analyses showed that the SNA predicted by $H_{n\text{-}open}$ correlated significantly with the actually measured SNA (r^2, 0.83; RMS, 13 a.u.; $P < 0.05$) (Fig. 6*B*), whereas the SNA predicted by $H_{n\text{-}closed\text{-}spon}$ showed no correlation (r^2, 0.04; RMS, 109 a.u.) (Fig. 6*C*). Using the data from all animals, the SNA predicted by $H_{n\text{-}open}$ correlated with the measured SNA (r^2, 0.8 ± 0.1; RMS, 15 ± 4 a.u.; $P < 0.05$), whereas SNA predicted by $H_{n\text{-}closed\text{-}spon}$ showed no correlation (r^2, 0.1 ± 0.1; RMS, 102 ± 24 a.u.).

In addition, the ability of the peripheral arc transfer functions (determined by protocols 1 and 2) to predict output dynamics (AP) from given input signals (SNA) in the open-loop condition was quantified by comparing with the actual measurements of AP response to SNA changes. Figure 7 shows an example obtained from the same animal as in Fig. 6. The AP response to SNA predicted by the open-loop transfer function ($H_{p\text{-}open}$) (third panel) resembled closely the actually measured AP (second panel). The AP response (bottom panels) predicted by the closed-loop-spontaneous transfer function ($H_{p\text{-}closed\text{-}spon}$) was also similar but with limitations. Scatter plot analyses showed that the AP predicted by $H_{p\text{-}open}$ correlated well with the measured AP (r^2, 0.75; RMS, 2 mmHg; $P < 0.05$; Fig. 7*B*), whereas the AP predicted by $H_{p\text{-}closed\text{-}spon}$ correlated partially with the measured values (r^2, 0.58; RMS, 3 mmHg; $P < 0.05$; Fig. 7*C*). Using the data from all animals, the $H_{p\text{-}open}$-predicted AP correlated well with the measured AP (r^2, 0.8 ± 0.1; RMS, 2 ± 2 mmHg; $P < 0.05$). The $H_{p\text{-}closed\text{-}spon}$-predicted AP similarly correlated with the measured AP, but with lower r^2 (0.7 ± 0.1) and higher RMS (3 ± 3 mmHg) compared with $H_{p\text{-}open}$ ($P < 0.05$).

Predictability of open-loop and closed-loop-spontaneous transfer functions compared with data measured in the closed-loop-spontaneous condition (protocol 4)

The ability of neural arc transfer functions (determined by protocols 1 and 2) to predict SNA from CSP input in the closed-loop-spontaneous condition was quantified by comparing with the actual SNA measurements in protocol 4. Figure 8 shows a typical example. Since CSP was matched with systemic AP, spontaneous fluctuation of AP was observed (Fig. 8*A*, top panel). AP increased spontaneously for 60–90 s but SNA did not decrease but increased, indicating that AP changes did not induce a negative SNA response via the baroreflex neural arc (Fig. 8*A*, third panel). Indeed, SNA predicted by $H_{n\text{-}open}$ (Fig. 8*A*, fourth panel) and

$H_{\text{n-closed-spon}}$ (Fig. 8*A*, bottom panel) were markedly different from the measured SNA (Fig. 8*A*, second and third panels). Scatter plot analyses indicated that these predicted SNAs did not correlate with the measured SNA (Fig. 8*B* and *C*).

In addition, the ability of peripheral arc transfer functions (determined by protocols 1 and 2) to predict AP from SNA input in the closed-loop-spontaneous condition was also quantified by comparing with the actually measured AP. Figure 9 shows a typical example obtained from the same animal as in Fig. 8. The spontaneous changes in SNA (Fig. 9*A*, second panel) appeared to precede those in AP (Fig. 9*A*, third panel), suggesting that SNA changes induced a positive response of AP via the baroreflex peripheral arc. Indeed, the AP (grey lines, re-sampled at 0.1 Hz) predicted by $H_{\text{p-open}}$ (Fig. 9*A*, fourth panel) and that predicted by $H_{\text{p-closed-spon}}$ (bottom panel) resembled the measured AP (third panel). Scatter plot analyses indicated that these predicted APs correlated well with the measured AP (Fig. 9*B* and *C*).

Similar results were found in all animals in the closed-loop-spontaneous resting condition. Changes in SNA always preceded alterations in AP, and induced a positive AP response. The closed-loop peripheral arc transfer function predicted the time series of AP dynamics with some degree of accuracy, whereas the neural arc transfer function failed to predict SNA.

Predictability of open-loop and closed-loop-spontaneous transfer functions compared with data measured during pharmacological pressure intervention in the closed-loop condition (protocol 5)

The ability of neural arc transfer functions (determined by protocols 1 and 2) to predict SNA from CSP change induced by pharmacological intervention under

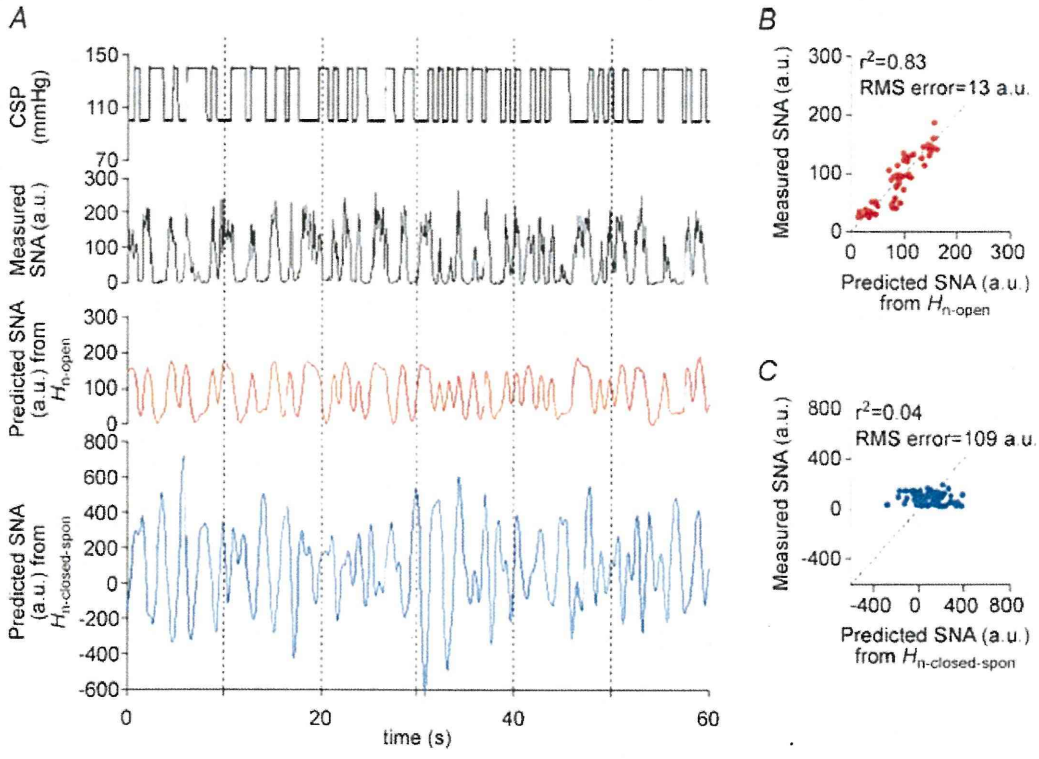

Figure 6. Predictability of neural arc transfer functions in open-loop condition
A, typical representative example of evaluating the predictability of SNA output from CSP input using the baroreflex transfer functions of the neural arc. The data were obtained from the same animal as in Fig. 3. The time-series SNA dynamics are predicted from CSP measured in protocol 4 (top panel), by the open-loop transfer function determined in protocol 1 (red line, third panel) and by the closed-loop-spontaneous transfer function determined in protocol 2 (blue line, bottom panel). CSP is changed according to a binary random (white-noise) signal with a switching interval of 500 ms under open-loop baroreflex condition. These predicted SNA changes are compared with the actual SNA measured in protocol 4 (second panel). SNA (red line, third panel) predicted by open-loop transfer function ($H_{\text{n-open}}$) appears to parallel the actually measured SNA, whereas SNA predicted by closed-loop-spontaneous transfer function ($H_{\text{n-closed-spon}}$) is markedly different from the measured SNA. *B*, scatter plot analysis of the SNA predicted by $H_{\text{n-open}}$ *versus* the measured SNA. *C*, scatter plot analysis of the SNA predicted by $H_{\text{n-closed-spon}}$ *versus* the measured SNA.

closed-loop conditions was quantified by comparing with the actual SNA measurements in protocol 5. The intervention was sequential bolus infusions of phenylephrine, nitroprusside and phenylephrine. Figure 10 shows a typical example. CSP was matched with systemic AP (Fig. 10*A*, first and second panels). The phenylephrine–nitroprusside–phenylephrine bolus infusions produced an increase–decrease–increase and recovery changes in AP, which led to changes in SNA as follows. When AP (which equals CSP) increased, actually measured SNA decreased, and vice versa (Fig. 10*A*, third panel).

The SNA response to CSP changes predicted by the open-loop transfer function ($H_{\text{n-open}}$) (Fig. 10*A*; fourth panel) resembled the actually measured SNA (third panel) in both the timing (phase) and intensity of neural activity. In contrast, the SNA response predicted by the closed-loop-spontaneous transfer function ($H_{\text{n-closed-spon}}$) (bottom panel) showed oppositely directed neural response as compared with actually measured SNA (third panel). When AP (which equals CSP) increased, the predicted SNA increased whereas the measured SNA decreased, and vice versa. As a result, scatter plot analyses showed that the SNA predicted by $H_{\text{n-open}}$ correlated significantly with the actually measured SNA (r^2, 0.87; RMS, 17 a.u.; $P < 0.05$; Fig. 10*B*), indicating a good predictability. However, the SNA predicted by $H_{\text{n-closed-spon}}$ showed negative correlation (r, −0.91; RMS, 114 a.u.; Fig. 10*C*), indicating a lack of predictability. The relationship between CSP (= AP) and actually measured SNA (Fig. 10*D* and *E*, open circles) was similar to that between CSP (= AP) and SNA predicted by $H_{\text{n-open}}$ (Fig. 10*D*, red circles) but different from that between CSP and SNA predicted by $H_{\text{n-closed-spon}}$ (Fig. 10*E*, blue circles). Using the data from all animals, the SNA predicted by $H_{\text{n-open}}$ correlated with the measured SNA (r^2, 0.9 ± 0.1; RMS, 16 ± 4 a.u.; $P < 0.05$), whereas SNA predicted by $H_{\text{n-closed-spon}}$ showed negative correlation (r, -0.8 ± 0.1; RMS, 112 ± 35 a.u.).

Discussion

Good predictability of open-loop baroreflex transfer functions

Although baroreflex transfer functions have been identified by open-loop analysis (Ikeda *et al.* 1996; Kawada *et al.* 2002; Kamiya *et al.* 2005*b*, 2008*a*), whether the

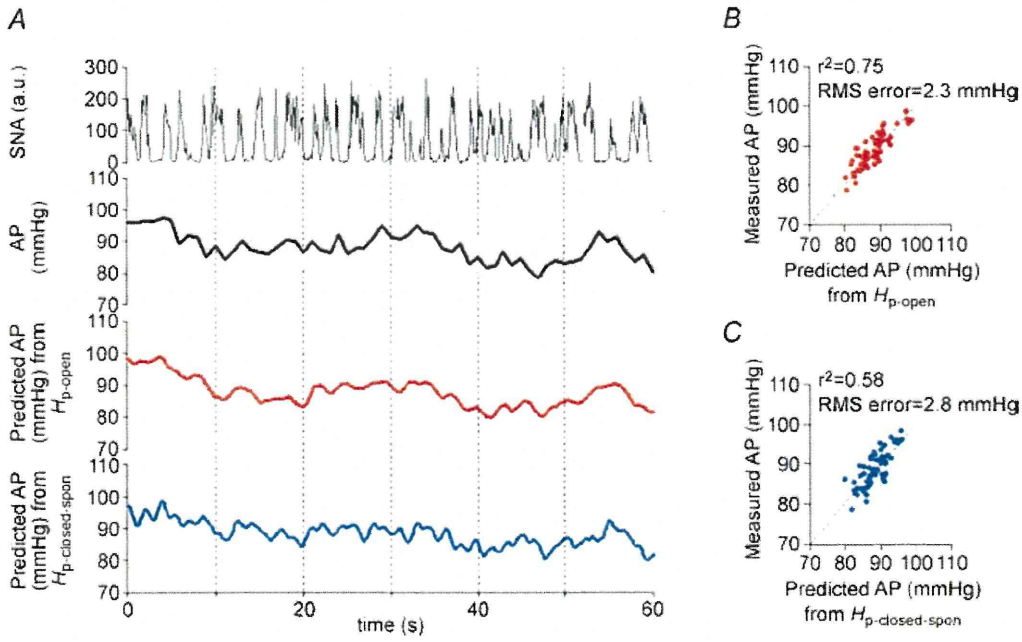

Figure 7. Predictability of peripheral arc transfer functions in open-loop condition
A, typical representative example of evaluating the predictability of AP output from SNA input using baroreflex transfer functions of the peripheral arc. The data were obtained from the same animal as in Fig. 3. The time-series AP dynamics are predicted from SNA measured in protocol 4 (top panel), by the open-loop transfer function determined in protocol 1 (red line, third panel) and by the closed-loop-spontaneous transfer function determined in protocol 2 (blue line, bottom panel). These predicted AP changes are compared with the actual AP measured in protocol 4 (the grey and black lines indicate AP re-sampled at 10 and 1 Hz, respectively; second panel). AP predicted by open-loop transfer function ($H_{\text{p-open}}$) appears to parallel the actually measured AP, whereas AP predicted by closed-loop-spontaneous transfer function ($H_{\text{n-closed-spon}}$) also correlates to some extent. *B*, scatter plot analysis of the AP predicted by $H_{\text{p-open}}$ *versus* the measured AP. *C*, scatter plot analysis of the AP predicted by $H_{\text{p-closed-spon}}$ *versus* the measured AP.

functions predict time-series output dynamics, which would confirm the accuracy of system identification of transfer function, remains to be elucidated. In the present study, we showed that the open-loop baroreflex transfer functions were able to predict output dynamics with high accuracy, even though the data set for determining the transfer functions (protocol 1) was different from that for investigating predictability (protocols 3, 4 and 5). The neural arc transfer function determined by the open-loop experiment ($H_{\text{n-open}}$) predicted SNA responses to measured CSP changes with r^2 of 0.8 ± 0.1. Likewise, the peripheral arc transfer function ($H_{\text{p-open}}$) also predicted the AP responses to measured SNA changes with r^2 of 0.8 ± 0.1 (Fig. 7). These results supported our first hypothesis that the open-loop baroreflex transfer functions for the neural and peripheral arcs are able to predict time-series SNA and AP outputs from baroreceptor pressure and SNA inputs, respectively. The good predictability indicates the accuracy of system identification of these transfer functions determined by open-loop experiments.

Inappropriate system identification and limited predictability of closed-loop spontaneous baroreflex transfer functions

Regarding the neural arc, our results showed that the transfer function determined under closed-loop-spontaneous conditions ($H_{\text{n-closed-spon}}$) was markedly different from that determined under open-loop conditions ($H_{\text{n-open}}$) (Fig. 5). In $H_{\text{n-closed-spon}}$, the increase in gain *versus* frequency was markedly enhanced (enhanced high-pass filter). A phase lead rather than phase lag indicates that the calculated phase may be incorrect since $H_{\text{n-open}}$ showed a linear phase lag, reflecting a fixed pure time delay from baroreceptor pressure to SNA (Orea *et al.* 2007). Furthermore, the step response of SNA to CSP predicted

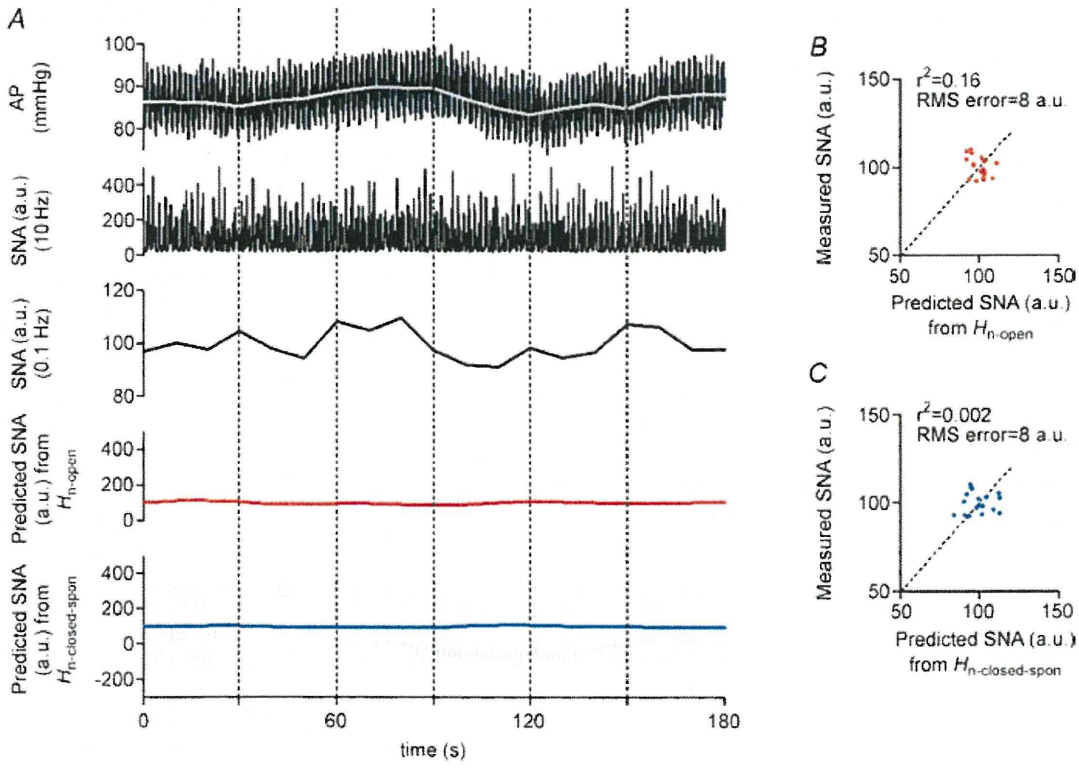

Figure 8. Predictability of neural arc transfer functions in closed-loop-spontaneous condition
A, example of spontaneous changes in AP (resampled at 10 and 0.1 Hz represented by black and grey lines, respectively, in the top panel) and SNA (re-sampled at 10 and 0.1 Hz in second and third panels, respectively) in closed-loop baroreflex condition (protocol 5). Using the open-loop ($H_{\text{n-open}}$, identified in protocol 1) and the closed-loop-spontaneous transfer functions ($H_{\text{n-closed-spon}}$, identified in protocol 2) of the neural arc, a time-series of SNA output was predicted from the actual AP measured in protocol 5. However, the predicted SNA (re-sampled at 10 Hz represented by grey line, and at 0.1 Hz represented by red and blue lines in fourth and bottom panels, respectively) response is markedly different from the trend of measured SNA. *B*, scatter plot analysis of the SNA predicted by $H_{\text{n-open}}$ *versus* the measured SNA. *C*, scatter plot analysis of the SNA predicted by $H_{\text{n-closed-spon}}$ *versus* the measured SNA.

by $H_{\text{n-closed-spon}}$ oscillated, although an initial decrease followed by partial recovery was predicted by $H_{\text{n-open}}$ (Fig. 5). These contradicting and strange characteristics of $H_{\text{n-closed-spon}}$ were associated with less appropriate predictability of time-series SNA output dynamics. Although the SNA predicted by $H_{\text{n-open}}$ in response to the measured changes in CSP was roughly similar to the actually measured SNA with respect to both amplitude and timing of the neural burst (Fig. 6*A* and *B*), the SNA predicted by $H_{\text{n-closed-spon}}$ was greatly different from the measured SNA, showing increased amplitude and inconsistent timing of neural burst (Fig. 6*A* and *C*). Therefore, with regard to the neural arc, these results support our second hypothesis that the closed-loop-spontaneous baroreflex transfer function is limited in its ability to predict the baroreflex dynamics compared with the open-loop transfer function.

Regarding the peripheral arc, however, the present study showed unexpected results. In contrast to the neural arc, the closed-loop-spontaneous baroreflex transfer function for the peripheral arc ($H_{\text{p-closed-spon}}$) approximated the open-loop transfer function ($H_{\text{p-open}}$) not only in gain and phase functions but also in the step response (Fig. 5). The similar characteristics of $H_{\text{p-closed-spon}}$ and $H_{\text{p-open}}$ yielded high predictability of time-series AP dynamics. The AP predicted by $H_{\text{p-closed-spon}}$ in response to the measured SNA changes was roughly the same as the actually measured AP (Fig. 7), although the correlation with measured data was lower than the AP predicted by $H_{\text{p-open}}$. Therefore, regarding the peripheral arc, these results support our second hypothesis and indicate that the closed-loop-spontaneous baroreflex transfer function is partially appropriate for system identification of the peripheral arc and is able to predict the time-series AP dynamics under resting conditions despite slightly limited accuracy compared with the open-loop transfer function. This finding may have great impact, because the closed-loop-spontaneous baroreflex transfer function has been believed to represent the neural arc function (Orea *et al.* 2007; Cooke *et al.* 2009; Ogoh *et al.* 2009).

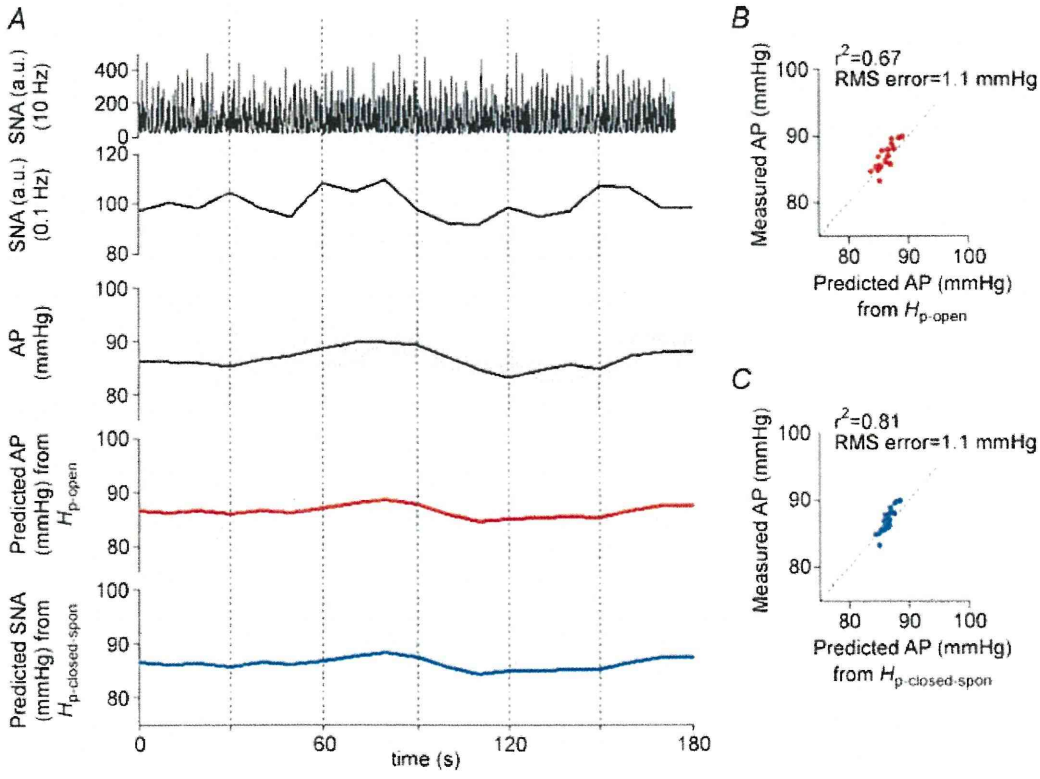

Figure 9. Predictability of peripheral arc transfer functions in closed-loop-spontaneous condition
A, example of spontaneous changes in SNA (re-sampled at 10 and 0.1 Hz in top and second panels, respectively) and AP (re-sampled at 10 and 0.1 Hz represented by grey and black lines, respectively, in third panel) under closed-loop baroreflex condition measured in protocol 5. Using the open-loop transfer function ($H_{\text{p-open}}$, identified in protocol 1) and the closed-loop-spontaneous transfer function ($H_{\text{p-closed-spon}}$, identified in protocol 2) of the peripheral arc, a time-series of AP output was predicted (re-sampled at 10 Hz represented by grey line, and at 0.1 Hz represented by red and blue lines in fourth and bottom panels, respectively) from the actual SNA measured in protocol 5. The predicted APs re-sampled at 0.1 Hz appear similar to the measured AP to some extent. *B*, scatter plot analysis of the AP predicted by $H_{\text{p-open}}$ *versus* the measured AP. *C*, scatter plot analysis of the AP predicted by $H_{\text{p-closed-spon}}$ *versus* the measured AP.

Potential mechanism for the limitation of closed-loop-spontaneous baroreflex transfer functions

It is indeed difficult to understand why the closed-loop-spontaneous transfer function is inappropriate for system identification of the neural arc but is partially appropriate for the peripheral arc. As a possible mechanism, we examined the effects of noise on the calculation of the closed-loop-spontaneous transfer function using numerical simulations (Fig. 11). Noise is considered as a factor that modulates output dynamics independent of input. Figure 11 (upper panels in *B*, *C* and *D*) shows block diagrams of the closed-loop baroreflex system. H_n represents central processing from baroreceptor pressure input to SNA, while H_p represents peripheral processing from SNA input to systemic AP. According to our previous studies (Ikeda *et al.* 1996; Kawada *et al.* 2002), we modelled H_n using derivative and high-cut filter characteristics with a pure delay, and H_p using second-order low-pass filter with a pure delay (see Appendix B, Fig. 11*A*) (Kamiya *et al.* 2005*b*). In this closed-loop baroreflex system, CSP equals AP. As noise, Gaussian white-noise was introduced to the neural and/or peripheral arcs (Fig. 1*C*). As in protocol 2, closed-loop-spontaneous transfer functions were calculated by the simplified method, from AP to SNA as the neural arc (corresponding to the $H_{n\text{-closed-spon}}$) and from SNA to AP as the peripheral arc (corresponding

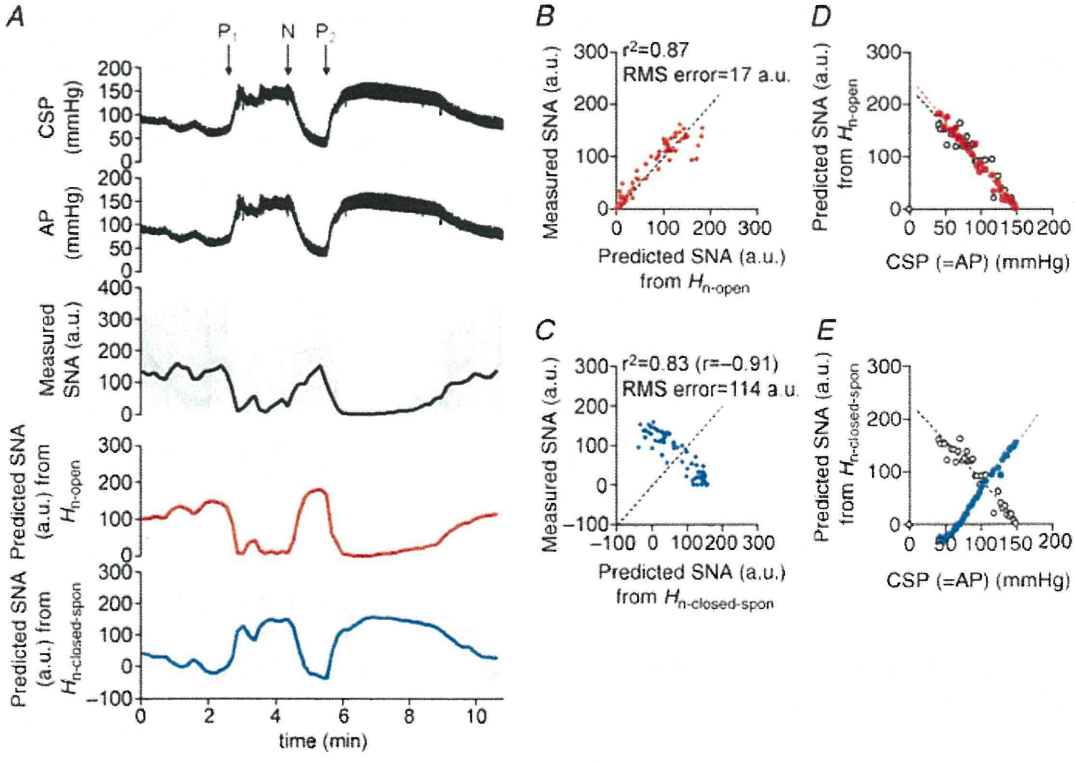

Figure 10. Predictability of neural arc transfer functions during pharmacological pressure interventions in closed-loop condition
A, example of changes in CSP and AP (re-sampled at 10 Hz in the top and second panels, respectively) induced by pharmacological interventions and SNA responses (re-sampled at 10 and 0.1 Hz represented by grey and black lines, respectively, in third panel) in closed-loop baroreflex condition (protocol 5). Sequential bolus infusions of phenylephrine (P_1), nitroprusside (N) and phenylephrine (P_2) were administered. Using the open-loop ($H_{n\text{-open}}$, identified in protocol 1) and the closed-loop-spontaneous transfer functions ($H_{n\text{-closed-spon}}$, identified in protocol 2) of the neural arc, time-series of SNA output was predicted (re-sampled at 10 Hz represented by grey line, and at 0.1 Hz represented by red and blue lines in fourth and bottom panels, respectively) from the actual AP measured in protocol 5. SNA predicted by open-loop transfer function ($H_{n\text{-open}}$) appears to parallel the actually measured SNA, whereas SNA predicted by closed-loop-spontaneous transfer function ($H_{n\text{-closed-spon}}$) is markedly different from the measured SNA. *B*, scatter plot analysis of the SNA predicted by $H_{n\text{-open}}$ *versus* the measured SNA. The identity line is shown. *C*, scatter plot analysis of the SNA predicted by $H_{n\text{-closed-spon}}$ *versus* the measured SNA. *D*, relationship between CSP and SNA predicted by $H_{n\text{-open}}$ (red filled circle, red broken line) is similar to that between CSP and actually measured SNA (open circle, black broken line) or *E*, relationship between CSP and SNA predicted by $H_{n\text{-closed-spon}}$ (blue filled circle, blue broken line) is different from that between CSP and actually measured SNA (open circle, black broken line).

to the $H_{p\text{-closed-spon}}$), while neglecting the noise (see Appendix A, Fig. 11*B*, *C* and *D*).

We next examined how the noise modifies the closed-loop-spontaneous transfer functions calculated by the simplified method and renders them different from the open-loop transfer functions by simulating three situations. Because of the closed-loop nature, changes in AP (thus, in CSP) modulate SNA via the neural arc transfer function (H_n), which in turn change AP via peripheral arc transfer function (H_p). In the first simulation, noise is present only in the neural arc (Fig. 11*B*). Regardless of the magnitude of the noise, the closed-loop-spontaneous transfer function for the neural arc is greatly different from the open-loop transfer function H_n (red lines), with markedly increased gain and phase lead *versus* frequency. In contrast, the closed-loop-spontaneous transfer function for the peripheral arc overlaps with the open-loop transfer function H_n. In the second simulation, noise is present only in the peripheral arc (Fig. 11*C*). Regardless of the magnitude of the noise, the closed-loop-spontaneous transfer function for the neural arc overlaps with the open-loop transfer function H_p, whereas that of the peripheral arc deviates markedly from the open-loop transfer function H_p (red

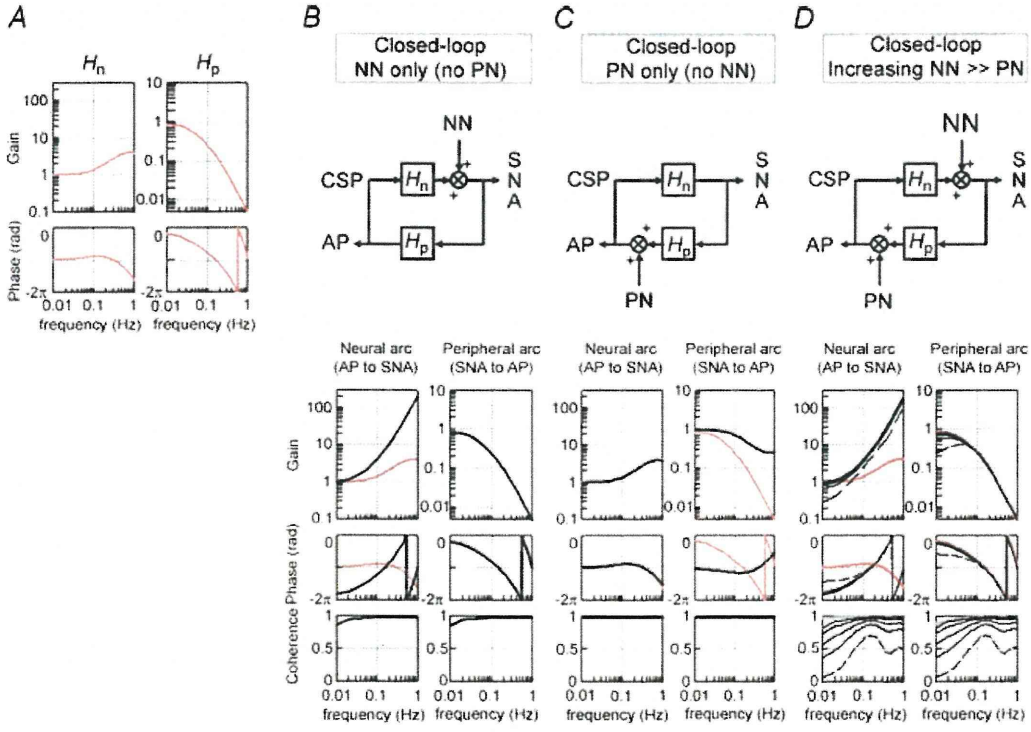

Figure 11. A numerical simulation of the effects of noise on calculation of baroreflex transfer functions
Noise (Gaussian white-noise) is introduced to the neural and/or peripheral arcs in closed-loop-spontaneous baroreflex condition, where CSP equals AP (see Figure 1*C*). *A*, the original baroreflex transfer functions of the neural (H_n, left panel) and peripheral (H_p, right panel) arcs. H_n is modelled using derivative and high-cut filter characteristics with a pure delay, and H_p using the second-order low-pass filter with a pure delay (see APPENDIX B). Units of gain are a.u. mmHg^{-1} for H_n and mmHg a.u.$^{-1}$ for H_p, respectively. *B–D*, block diagrams (upper panels) and closed-loop-spontaneous transfer functions (lower panels); calculated from AP to SNA as the neural arc (left lower panel) and from SNA to AP as the peripheral arc (right lower panel). The open-loop transfer functions (H_n, H_p) are included as reference (gray lines). Units of gain are a.u. mmHg^{-1} for the neural arc and mmHg a.u.$^{-1}$ for the peripheral arc, respectively. *B*, first simulation: noise (0.029, 0.117, 0.264, 0.732 and 2.928 × 10^3 au^2) is present only in the neural arc. The same results are obtained irrespective of the noise intensity. The closed-loop-spontaneous transfer function of the neural arc is totally different from the open-loop transfer function H_n, whereas that of the peripheral arc overlaps with H_p. C: Second simulation: noise (0.029, 0.117, 0.264, 0.732 and 2.928 × 10^3 mmHg^2 is present only in the peripheral arc. The same results are obtained irrespective of the noise intensity. The closed-loop-spontaneous transfer function of the neural arc overlaps the open-loop transfer function H_n, whereas that of the peripheral arc is markedly different from H_n. *D*, third simulation: noise with incremental intensity [from 0.029 (broken line) to 0.117, 0.264, 0.732 and 2.928 (solid lines) × 10^3 au^2] is present in the neural arc, while a small constant noise (29 mmHg^2) is present in the peripheral arc. The closed-loop-spontaneous transfer function of the neural arc is different from the open-loop transfer function of H_n, whereas that of the peripheral arc approaches H_p and the two become overlapped as the noise in the neural arc increases. H_n, neural arc transfer function; H_p, peripheral arc transfer function, NN, unknown neural noise; PN, unknown peripheral noise.

lines). In the third simulation, an incremental noise is present in the neural arc and a small constant noise in the peripheral arc (Fig. 11*D*). Regardless of the magnitude of the noise, the closed-loop-spontaneous transfer function for the neural arc is different from the open-loop transfer function H_n (red lines). However, as the noise in the neural arc increases, the closed-loop-spontaneous transfer function for the peripheral arc approaches the open-loop transfer function H_p and becomes superimposed with respect to gain, phase and coherence functions. These simulations indicate that the presence of noise in the neural and peripheral arcs reduces the accuracy of identification of closed-loop-spontaneous transfer function for the neural and peripheral arc, respectively. Importantly, our experimental results (Fig. 5) may be consistent with the situation that noise is predominant in the neural arc rather than in the peripheral arc (Fig. 11*B* and *D*). This might reflect our experimental condition that had little or no noise in the peripheral arc (i.e. perturbation to AP), probably because the body did not move in closed-loop baroreflex and spontaneous resting conditions. Therefore, a noise predominantly in the neural arc may be a potential mechanism responsible for our experimental finding that the closed-loop-spontaneous transfer function is inappropriate in identifying the neural arc but partially appropriate in identifying the peripheral arc under resting conditions.

Physiological implication (1): Baroreflex is predominantly feedforward rather than feedback in the closed-loop-spontaneous condition

While we separate the total arc (CSP input to systemic AP) of the baroreflex system into the neural (CSP input to SNA) and peripheral (SNA input to systemic AP) arc subsystems, the neural and the peripheral arcs are equivalent to the feedback and feedforward arcs, respectively, as reported in earlier studies (Barres *et al.* 2004; Brychta *et al.* 2007). Using these terms, our data indicate that the baroreflex loop is predominantly feedforward rather than feedback in the closed-loop-spontaneous resting condition. This may be explained by the block diagram and simulation results shown in Fig. 11*D*. As the noise in the neural arc increases, SNA fluctuates more but becomes less dependent on CSP (baroreceptor pressure input), while the augmented SNA changes strongly the control systemic AP via the peripheral arc transfer function (H_p) with little interruption by noise in the peripheral arc. As a result, baroreflex control becomes feedforward-like, while the closed-loop-spontaneous transfer function for the peripheral arc approaches the open-loop transfer function H_p. This concept may explain our findings that the closed-loop-spontaneous baroreflex transfer function for the peripheral arc partially matched the open-loop transfer function, whereas that for the neural arc did not (Fig. 5). In addition, this concept may also explain other data that in the closed-loop-spontaneous condition, spontaneous changes in SNA appeared to precede changes in AP and induce positive AP responses (Fig. 9*A*), and that the closed-loop-spontaneous peripheral arc transfer function was capable of predicting the time-series AP dynamics from SNA (Fig. 9*B* and *C*).

Physiological implication (2): Potential mechanisms for AP and SNA fluctuations in the closed-loop-spontaneous condition

Our experiments of opening and closing the baroreflex loop in individual animals may help to suggest potential mechanisms responsible for AP and SNA fluctuations in the closed-loop condition. First, both SNA auto-rhythmicity (pacemaker) and baroreflex mechanisms may contribute to fluctuations of AP and SNA at approximately 0.4 Hz actually observed in the closed-loop-spontaneous baroreflex condition (Fig. 4*B*), which is often termed the Mayer wave (Malpas & Burgess, 2000; Barres *et al.* 2004). It is noteworthy that even in the baroreflex open-loop condition, the SNA autospectrum shows a small peak at approximately 0.4 Hz (arrowhead, Fig. 3*B*) despite no peak in CSP autospectrum, indicating the existence of SNA auto-rhythmicity at 0.4 Hz, which in turn produces systemic AP fluctuation at that frequency (Fig. 3*B*) via peripheral arc transfer function (Fig. 3*C*). This may explain the coherence drop at approximately 0.4 Hz (from CSP to SNA) in open-loop condition (Fig. 3*C*). Furthermore, since closing the baroreflex loop greatly increases the peak of the SNA autospectrum (arrowhead, Fig. 4*B*), interaction between the baroreflex neural and peripheral arcs is important for these fluctuations. This may be consistent with the report that bilateral denervation of aortic and carotid sinus baroreceptors eliminated 0.4 Hz oscillations of AP and SNA during sympathoexcitatory stress (Barres *et al.* 2004). Collectively, SNA auto-rhythmicity (which equals 'origin' activity) and its development and propagation by the baroreflex may partly be responsible for the 0.4 Hz fluctuations of AP and SNA in this experimental condition.

Second, although the baroreflex feedback system can theoretically generate oscillations of AP and SNA by itself without other factors (i.e. SNA auto-rhythmicity) in the closed-loop condition (Guyton & Harris, 1951; deBoer *et al.* 1987; Kamiya *et al.* 2005*a*), the baroreflex loop theory might not contribute to the 0.4 Hz AP and SNA fluctuations observed in the closed-loop-spontaneous condition, for the following reason. The key point of the baroreflex loop theory is that when the gain of total arc baroreflex transfer function is greater than 1 at the

frequency where the phase reaches -2π radians (which we define as f_0), oscillations of AP and SNA will occur at around f_0. In our actual data, f_0 was approximately 0.13 Hz (Fig. 3*E*), which is consistent with a previous study (Malpas & Burgess, 2000) showing increased 0.1 Hz oscillation of AP during haemorrhage in rabbits. Moreover, the gain at f_0 was less than 1 (Fig. 3*E*), indicating no oscillations generated according to the baroreflex loop theory. Therefore, in the closed-loop-spontaneous condition, the baroreflex loop theory would not contribute to the 0.4 Hz fluctuations of AP and SNA.

Lastly, respiratory-mediated fluctuation of AP may contribute to SNA fluctuation via baroreflex mechanisms. In the baroreflex open-loop condition (Fig. 3*B*), SNA autospectrum shows no peak whereas systemic AP shows a large peak at the frequency of artificial respiration (approximately 0.57 Hz) (Fig. 3*B*). This indicates that AP fluctuation at that frequency is not mediated by SNA but by mechanical aspects of respiration (i.e. respiratory changes in intrathoracic pressure), consistent with an earlier report (Brychta *et al.* 2007). Since closing the baroreflex loop produces a peak in the SNA autospectrum at the respiratory frequency (Fig. 4*B*), a baroreflex mechanism may partly be responsible for respiratory-mediated SNA fluctuation in this experimental condition.

Physiological implication (3): open-loop baroreflex neural arc transfer function is able to predict closed-loop time-series SNA response to drug-induced AP change

The data discussed so far were obtained using mechanical interventions to change carotid sinus pressure, which arguably are not physiological changes. To validate whether the predictabilities of the open-loop and closed-loop-spontaneous transfer functions apply to more physiological conditions, we tested the neural arc transfer functions using pharmacological pressure intervention (phenylephrine and nitroprusside infusions) under closed-loop conditions. First, the SNA predicted by the open-loop baroreflex neural arc transfer function ($H_{\text{n-open}}$) in response to the measured changes in CSP (= AP) was roughly similar to the actually measured SNA with respect to both amplitude and timing of neural activity (Fig. 10*A*, third and fourth panel), showing high correlation ($r^2 = 0.9$, Fig. 10*B*). This result indicates that with regard to the neural arc, the open-loop transfer function is able to predict time-series SNA output from AP input even during pharmacological pressure interventions. A possible explanation for the good predictability is that since the pharmacological interventions exert a noise to the peripheral and not the neural arc, time-series SNA is almost determined by the pharmacologically induced changes in baroreceptor pressure (= systemic AP) via the neural arc transfer function (= $H_{\text{n-open}}$).

In contrast to the open-loop transfer function, the SNA predicted by the closed-loop-spontaneous baroreflex neural arc transfer function ($H_{\text{n-closed-spon}}$) was different from the measured SNA. The predicted SNA was an oppositely directed neural response: when AP (= CSP) increased, the predicted SNA increased whereas the measured SNA decreased, and vice versa. Therefore, with regard to the neural arc, the closed-loop-spontaneous transfer function is not able to predict SNA dynamics from AP. The failure in predicting SNA change may be explained by inappropriate system identification in the closed-loop condition. Because of the closed-loop condition, the calculated phase function of $H_{\text{n-closed-spon}}$ was the inverse of that of $H_{\text{p-closed-spon}}$. Indeed, the phase led as frequency increased (Figs 5, 11*B* and *D*) in contrast to the phase lag of the open-loop transfer function ($H_{\text{n-open}}$). Furthermore, the calculated phase of $H_{\text{n-closed-spon}}$ resulted in an oppositely directed response of predicted SNA as compared with actually measured SNA, in contrast to the good match of predicted SNA by $H_{\text{n-open}}$. These results indicate that with regard to the neural arc, the open-loop neural arc transfer function predicts time-series SNA response to changes in AP induced by pharmacological interventions, while the closed-loop-spontaneous transfer function cannot predict SNA response.

Although spontaneous baroreflex measures are believed to represent the neural arc function (baroreflex control of SNA), the present study raises potential methodological issues. First, since the baroreflex is a closed-loop feedback system, there is theoretical difficulty in identifying system characteristics in the closed-loop spontaneous condition. Since a relationship calculated from SNA input to AP during their spontaneous fluctuations is the inverse of that calculated from AP input to SNA, the calculation itself cannot determine the causality between them. Our present data clearly indicate limitation in estimating closed-loop-spontaneous transfer function of the neural arc, and that a good estimation requires opening the loop and introducing an intervention to the loop. Furthermore, although the spontaneous baroreflex transfer function obtained in the closed-loop condition (Orea *et al.* 2007; Cooke *et al.* 2009; Ogoh *et al.* 2009) has been used as a surrogate for the neural (feedback) arc function of the baroreflex loop, it actually represents the peripheral (feedforward) arc function since baroreflex loop is predominantly feedforward rather than feedback in the closed-loop-spontaneous condition.

Second, a recent study (Hart *et al.* 2010) has reported that spontaneous baroreflex measures (slope of strength of muscle SNA burst over-binned or non-binned AP) did not correlate ($r^2 = 0.05$–0.13) with the 'gold standard' modified Oxford analysis (nitroprusside and phenylephrine), whereas spontaneous threshold measure

(slope of % occurrence of muscle SNA burst over 1 mmHg binned AP, eliminating strength of SNA burst) correlated with it mildly ($r^2 = 0.5$). Although we cannot directly compare the transfer function analysis in our present study with the spontaneous threshold measure reported by Hart *et al.* (2010) because of methodological differences, our open-loop transfer function of the neural arc was able to predict occurrence and magnitude of time-series SNA with a higher degree of accuracy ($r^2 = 0.9$, Fig. 10*B*) and reproduce the AP–SNA relationship during closed-loop, drug-induced AP changes (Fig. 10*D*).

Limitations

The present study has several limitations. First, we excluded the efferent effect of the vagally mediated arterial baroreflex, which could affect the properties of baroreflex control of SNAs. Second, artificial respiration and surgical procedures used in this study could affect baroreflex. Third, anaesthetic agents tend to inhibit efferent SNA and depress the gain of baroreflex control of SNA. Fourth, since the present study was animal research, it is limited in its applicability to humans. However, a problem of difficulty in identifying the 'closed-loop' system in contrast with the 'open-loop' system is common in animal and human studies. Lastly, we perfused the carotid sinuses with physiological saline pre-equilibrated with atmospheric. Local hypoxia could have occurred and somewhat affected baroreflex control of SNA. Further research to examine the relevance of the present findings to true physiological conditions is necessary.

Summary

In summary, the open-loop baroreflex transfer functions for the neural and peripheral arcs allowed good prediction of the time-series SNA and AP outputs from baroreceptor pressure and SNA inputs, respectively. In contrast, the closed-loop-spontaneous baroreflex transfer function for the neural arc deviated greatly from the open-loop transfer function, and could not predict the time-series SNA dynamics. However, the closed-loop-spontaneous baroreflex transfer function for the peripheral arc partially matched the open-loop transfer function, with reasonable predictability of the time-series AP dynamics although slightly inferior in accuracy. Furthermore, the predictabilities of open-loop and closed-loop-spontaneous transfer functions of the neural arc were validated by closed-loop pharmacological (phenylephrine and nitroprusside infusions) pressure interventions. Time-series SNA responses to drug-induced AP changes predicted by the open-loop transfer function matched closely the measured responses, whereas SNA responses predicted by the closed-loop-spontaneous transfer function deviated greatly and were the inverse of measured responses. Therefore, although the spontaneous baroreflex transfer function obtained by closed-loop analysis has been believed to represent the neural arc function, it is inappropriate for system identification of the neural arc but is partially appropriate for system identification of the peripheral arc under resting condition, compared with open-loop analysis.

Appendix A

In a block diagram of the open-loop baroreflex system (Fig. 1*A*), CSP is independent of systemic AP because of vascular isolation of the carotid-sinus regions. In this framework, input–output relationships of these arcs are expressed in the frequency domain as:

$$\mathrm{SNA}(f) = H_\mathrm{n}(f) \cdot \mathrm{CSP}(f) + \mathrm{NN}(f) \quad \text{(A1)}$$

$$\mathrm{AP}(f) = H_\mathrm{p}(f) \cdot \mathrm{SNA}(f) + \mathrm{PN}(f) \quad \text{(A2)}$$

where CSP(f), SNA(f) and AP(f) are the fast Fourier transforms of CSP, SNA and systemic AP, respectively. $H_\mathrm{n}(f)$ and $H_\mathrm{p}(f)$ denote the neural arc and the peripheral arc transfer functions, respectively. NN(f) and PN(f) represent unknown noise in the neural and peripheral arcs, respectively.

In the neural arc, calculating the ensemble averages of cross-powers between the terms of eqn (A1) and CSP(f) yields

$$E[\mathrm{SNA}(f) \cdot \mathrm{CSP}(f)^*] = H_\mathrm{n}(f) \cdot E[\mathrm{CSP}(f) \cdot \mathrm{CSP}(f)^*] + E[\mathrm{NN}(f) \cdot \mathrm{CSP}(f)^*] \quad \text{(A3)}$$

where $E[\,]$ indicates an ensemble average operation. CSP(f)* denotes the complex conjugate of CSP(f). As $H_\mathrm{n}(f)$ is supposed to be time invariant during the observation period, $H_\mathrm{n}(f)$ is outside the ensemble average operation. When CSP is a white-noise signal, E[NN(f)·CSP(f)*] diminishes to zero asymptotically because the white noise is statistically independent of any other noise signal. Thus, we can estimate $H_\mathrm{n}(f)$ by the following equation, which we designate $H_\mathrm{n\text{-}open}(f)$.

$$H_\mathrm{n}(f) = \frac{E[\mathrm{SNA}(f) \cdot \mathrm{CSP}(f)^*]}{E[\mathrm{CSP}(f) \cdot \mathrm{CSP}(f)^*]} = H_\mathrm{n\text{-}open}(f) \quad \text{(A4)}$$

Similarly, in the peripheral arc, calculating ensemble averages of cross-powers between terms of eqn (A2) and SNA(f) yields

$$E[\mathrm{AP}(f) \cdot \mathrm{SNA}(f)^*] = H_\mathrm{p}(f) \cdot E[\mathrm{SNA}(f) \cdot \mathrm{SNA}(f)^*] + E[\mathrm{PN}(f) \cdot \mathrm{SNA}(f)^*] \quad \text{(A5)}$$

where SNA(f)* denotes the complex conjugate of SNA(f). As $H_\mathrm{p}(f)$ is supposed to be time invariant during the

observation period, $H_p(f)$ is outside the ensemble average operation. In the open-loop condition, since PN(f) cannot affect SNA(f) and is statistically independent of SNA(f) by definition, $E[\mathrm{PN}(f)\cdot\mathrm{SNA}(f)^*]$ diminishes to zero asymptotically. Thus, we can estimate $H_p(f)$ by the following equation, which we designate $H_{\text{p-open}}(f)$.

$$H_p(f) = \frac{E[\mathrm{AP}(f)\cdot\mathrm{SNA}(f)^*]}{E[\mathrm{SNA}(f)\cdot\mathrm{SNA}(f)^*]} = H_{\text{p-open}}(f) \tag{A6}$$

In contrast to the open-loop condition, CSP is matched with systemic AP in the closed-loop-spontaneous baroreflex condition (Fig. 1*B*). Thus, the input–output relationships of the arcs in the frequency domain are expressed as:

$$\mathrm{SNA}(f) = H_n(f)\cdot\mathrm{AP}(f) + \mathrm{NN}(f) \tag{A7}$$

$$\mathrm{AP}(f) = H_p(f)\cdot\mathrm{SNA}(f) + \mathrm{PN}(f) \tag{A8}$$

In the neural arc, calculating ensemble averages of cross-powers between the terms of eqn (A7) and AP(f) yields

$$E[\mathrm{SNA}(f)\cdot\mathrm{AP}(f)^*] = H_n(f)\cdot E[\mathrm{AP}(f)\cdot\mathrm{AP}(f)^*] + E[\mathrm{NN}(f)\cdot\mathrm{AP}(f)^*] \tag{A9}$$

$$H_n(f) = \frac{E[\mathrm{SNA}(f)\cdot\mathrm{AP}(f)^*]}{E[\mathrm{AP}(f)\cdot\mathrm{AP}(f)^*]} - \frac{E[\mathrm{NN}(f)\cdot\mathrm{AP}(f)^*]}{E[\mathrm{AP}(f)\cdot\mathrm{AP}(f)^*]} \tag{A10}$$

However, in the baroreflex closed-loop conditions, the unknown noise in SNA (NN) can affect AP through the peripheral arc transfer function (H_p). In other words, AP(f) inevitably correlates with NN(f), and $E[\mathrm{NN}(f)\cdot\mathrm{AP}(f)^*]$ does not diminish to zero. $H_n(f)$ cannot be determined because the unknown noise NN is practically impossible to quantify. Therefore in protocol 3, we simplify eqn (A10) by neglecting the last term, and define the closed-loop-spontaneous transfer function by the following equation, which we designate $H_{\text{n-closed-spon}}(f)$.

$$H_n(f) = \frac{E[\mathrm{SNA}(f)\cdot\mathrm{AP}(f)^*]}{E[\mathrm{AP}(f)\cdot\mathrm{AP}(f)^*]} = H_{\text{n-closed-spon}}(f) \tag{A11}$$

However, from eqns (A4) and (A11), it is evident that $H_{\text{n-closed-spon}}(f)$ should be different from $H_{\text{n-open}}(f)$ when NN(f) is large and cannot be neglected.

In the peripheral arc, calculating ensemble averages of cross-powers between the terms of eqn (A8) and SNA(f) yields:

$$E[\mathrm{AP}(f)\cdot\mathrm{SNA}(f)^*] = H_p(f)\cdot E[\mathrm{SNA}(f)\cdot\mathrm{SNA}(f)^*] + E[\mathrm{PN}(f)\cdot\mathrm{SNA}(f)^*] \tag{A12}$$

$$H_p(f) = \frac{E[\mathrm{AP}(f)\cdot\mathrm{SNA}(f)^*]}{E[\mathrm{SNA}(f)\cdot\mathrm{SNA}(f)^*]} - \frac{E[\mathrm{PN}(f)\cdot\mathrm{SNA}(f)^*]}{E[\mathrm{SNA}(f)\cdot\mathrm{SNA}(f)^*]} \tag{A13}$$

However, in the baroreflex closed-loop conditions, the unknown noise in AP (PN) can affect SNA through the neural arc transfer function (H_n). In other words, SNA(f) inevitably correlates with PN(f), and $E[\mathrm{PN}(f)\cdot\mathrm{SNA}(f)^*]$ does not diminish to zero. $H_p(f)$ cannot be determined because the unknown noise PN is practically impossible to quantify. Therefore in protocol 3, we simplify eqn (A13) by neglecting the last term and define the closed-loop-spontaneous transfer function by the following equation, which we designate $H_{\text{p-closed-spon}}(f)$.

$$H_p(f) = \frac{E[\mathrm{AP}(f)\cdot\mathrm{SNA}(f)^*]}{E[\mathrm{SNA}(f)\cdot\mathrm{SNA}(f)^*]} = H_{\text{p-closed-spon}}(f) \tag{A14}$$

However, from eqns (A6) and (A14), it is evident that $H_{\text{p-closed-spon}}(f)$ should be different from $H_{\text{p-open}}(f)$ when PN(f) is large and cannot be neglected.

Appendix B

In rabbits, the transfer function of the baroreflex neural arc (baroreceptor pressure/CSP to SNA) approximates derivative characteristics in the frequency range below 0.8 Hz, and high-cut characteristics of frequencies above 0.8 Hz (Kawada *et al.* 2002). Therefore, according to our previous study, we model the neural arc transfer function (H_n) using eqn (B1) as follows

$$H_n(f) = -K_n \frac{1 + \frac{f}{f_{c1}}j}{\left(1 + \frac{f}{f_{c2}}\right)^2} \exp(-2\pi f j L) \tag{B1}$$

where f and j represent the frequency (in Hz) and imaginary units, respectively; K_n is static gain (in a.u. mmHg^{-1}); f_{c1} and f_{c2} ($f_{c1} < f_{c2}$) are corner frequencies (in Hz) for derivative and high-cut characteristics, respectively; and L is a pure delay (in s), that would represent the sum of delays in synaptic transmission in the baroreflex central pathways and the sympathetic ganglion. The dynamic gain increases in the frequency range from f_{c1} to f_{c2}, and decreases above f_{c2}. Based on the measured results, we set K_n, f_{c1}, f_{c2} and L at 1, 0.1, 0.8 and 0.2, respectively, in all simulations in Fig. 11.

In addition, the transfer function of the baroreflex peripheral arc (SNA to systemic AP) approximates the second-order low-pass filter with a lag time in rabbits (Kawada *et al.* 2002). Therefore, we model the peripheral

arc transfer function (H_p) using eqn (B2) as follows:

$$H_p(f) = \frac{K_p}{1 + 2\zeta\frac{f}{f_N}j + \left(\frac{f}{f_N}j\right)^2} \exp(-2\pi f j L) \quad \text{(B2)}$$

where K_p is static gain (in mmHg a.u.$^{-1}$); fN and ζ indicate a natural frequency (in Hz) and a damping ratio, respectively; and L is a pure delay (in s) that would represent the sum of delays in synaptic transmission in the neuroeffector junction and intracellular signal transduction in the effector organs. Based on the measured results, we set K_p, f_N, ζ and L at 1, 0.07, 1.4 and 1.0, respectively, in all simulations in Fig. 11.

References

Barres C, Cheng Y & Julien C (2004). Steady-state and dynamic responses of renal sympathetic nerve activity to air-jet stress in sinoaortic denervated rats. *Hypertension* **43**, 629–635.

Brychta RJ, Shiavi R, Robertson D, Biaggioni I & Diedrich A (2007). A simplified two-component model of blood pressure fluctuation. *Am J Physiol Heart Circ Physiol* **292**, H1193–H1203.

Cooke WH, Hoag JB, Crossman AA, Kuusela TA, Tahvanainen KU & Eckberg DL (1999). Human responses to upright tilt: a window on central autonomic integration. *J Physiol* **517**, 617–628.

Cooke WH, Rickards CA, Ryan KL, Kuusela TA & Convertino VA (2009). Muscle sympathetic nerve activity during intense lower body negative pressure to presyncope in humans. *J Physiol* **587**, 4987–4999.

deBoer RW, Karemaker JM & Strackee J (1987). Hemodynamic fluctuations and baroreflex sensitivity in humans: a beat-to-beat model. *Am J Physiol Heart Circ Physiol* **253**, H680–H689.

DiBona GF & Sawin LL (2003). Frequency response of the renal vasculature in congestive heart failure. *Circulation* **107**, 2159–2164.

DiBona GF & Sawin LL (2004). Effect of renal denervation on dynamic autoregulation of renal blood flow. *Am J Physiol Renal Physiol* **286**, F1209–F1218.

Drummond GB (2009). Reporting ethical matters in *The Journal of Physiology*: standards and advice. *J Physiol* **587**, 713–719.

Eckberg DL & Sleight P (1992). *Human Baroreflexes in Health and Disease*. Oxford University Press, New York.

Guyton A & Harris J (1951). Pressoreceptor-autonomic oscillation: a probable cause of vasomotor waves. *Am J Physiol* **165**, 158–166.

Hart EC, Joyner MJ, Wallin BG, Karlsson T, Curry TB & Charkoudian N (2010). Baroreflex control of muscle sympathetic nerve activity: a nonpharmacological measure of baroreflex sensitivity. *Am J Physiol Heart Circ Physiol* **298**, H816–H822.

Ikeda Y, Kawada T, Sugimachi M, Kawaguchi O, Shishido T, Sato T *et al.* (1996). Neural arc of baroreflex optimizes dynamic pressure regulation in achieving both stability and quickness. *Am J Physiol Heart Circ Physiol* **271**, H882–H890.

Ikeda Y, Sugimachi M, Yamasaki T, Kawaguchi O, Shishido T, Kawada T *et al.* (1995). Explorations into development of a neurally regulated cardiac pacemaker. *Am J Physiol Heart Circ Physiol* **269**, H2141–H2146.

Julius SB & Allan GP (ed.) (2000). *Random Data: Analysis and Measurement Procedures*. John Wiley & Sons, Inc., New York.

Kamiya A, Hayano J, Kawada T, Michikami D, Yamamoto K, Ariumi H *et al.* (2005*a*). Low-frequency oscillation of sympathetic nerve activity decreases during development of tilt-induced syncope preceding sympathetic withdrawal and bradycardia. *Am J Physiol Heart Circ Physiol* **289**, H1758–H1769.

Kamiya A, Kawada T, Mizuno M, Shimizu S & Sugimachi M (2010). Parallel resetting of arterial baroreflex control of renal and cardiac sympathetic nerve activities during upright tilt in rabbits. *Am J Physiol Heart Circ Physiol* **298**, H1966–H1975.

Kamiya A, Kawada T, Yamamoto K, Michikami D, Ariumi H, Miyamoto T *et al.* (2005*b*). Dynamic and static baroreflex control of muscle sympathetic nerve activity (SNA) parallels that of renal and cardiac SNA during physiological change in pressure. *Am J Physiol Heart Circ Physiol* **289**, H2641–H2648.

Kamiya A, Kawada T, Yamamoto K, Mizuno M, Shimizu S & Sugimachi M (2008*a*). Upright tilt resets dynamic transfer function of baroreflex neural arc to minify the pressure disturbance in total baroreflex control. *J Physiol Sci* **58**, 189–198.

Kamiya A, Michikami D, Iwase S & Mano T (2008*b*). Decoding rule from vasoconstrictor skin sympathetic nerve activity to nonglabrous skin blood flow in humans at normothermic rest. *Neurosci Lett* **439**, 13–17.

Kawada T, Li M, Kamiya A, Shimizu S, Uemura K, Yamamoto H & Sugimachi M (2010). Open-loop dynamic and static characteristics of the carotid sinus baroreflex in rats with chronic heart failure after myocardial infarction. *J Physiol Sci* **60**, 283–298.

Kawada T, Zheng C, Yanagiya Y, Uemura K, Miyamoto T, Inagaki M *et al.* (2002). High-cut characteristics of the baroreflex neural arc preserve baroreflex gain against pulsatile pressure. *Am J Physiol Heart Circ Physiol* **282**, H1149–H1156.

Malpas SC & Burgess DE (2000). Renal SNA as the primary mediator of slow oscillations in blood pressure during hemorrhage. *Am J Physiol Heart Circ Physiol* **279**, H1299–H1306.

Ogoh S, Fisher JP, Young CN, Raven PB & Fadel PJ (2009). Transfer function characteristics of the neural and peripheral arterial baroreflex arcs at rest and during postexercise muscle ischemia in humans. *Am J Physiol Heart Circ Physiol* **296**, H1416–H1424.

Orea V, Kanbar R, Chapuis B, Barres C & Julien C (2007). Transfer function analysis between arterial pressure and renal sympathetic nerve activity at cardiac pacing frequencies in the rat. *J Appl Physiol* **102**, 1034–1040.

Rowell LB (1993). *Human Cardiovascular Control*. Oxford University Press, New York.

Zhang R, Zuckerman JH, Iwasaki K, Wilson TE, Crandall CG & Levine BD (2002). Autonomic neural control of dynamic cerebral autoregulation in humans. *Circulation* **106**, 1814–1820.

Author contributions

The experiments were performed at the Department of Cardiovascular Dynamics, National Cerebral and Cardiovascular Center Research Institute. A.K. absolutely contributed to: (1) Conception and design, (2) Collection, analysis and interpretation of data and (3) Drafting the article or revising it critically for important intellectual content. Other authors helped him particularly in (3). All authors approved the final version.

Acknowledgments

This study was supported by a research project promoted by Ministry of Health, Labour and Welfare in Japan (no. H21-nano-ippan-005, H22-nanchi-ippan-142), the Grants-in-Aid for Scientific Research promoted by Ministry of Education, Culture, Sports, Science and Technology in Japan (no. 20390462, 22791559) and the Industrial Technology Research Grant Program from New Energy and Industrial Technology Development Organization (NEDO) of Japan.

Am J Physiol Regul Integr Comp Physiol 300: R969–R977, 2011.
First published January 26, 2011; doi:10.1152/ajpregu.00768.2010.

Exercise training augments the dynamic heart rate response to vagal but not sympathetic stimulation in rats

Masaki Mizuno,[1,2] Toru Kawada,[2] Atsunori Kamiya,[2] Tadayoshi Miyamoto,[2,3] Shuji Shimizu,[2] Toshiaki Shishido,[2] Scott A. Smith,[1] and Masaru Sugimachi[2]

[1]*Departments of Physical Therapy and Internal Medicine, University of Texas Southwestern Medical Center at Dallas, Dallas, Texas;* [2]*Department of Cardiovascular Dynamics, National Cerebral and Cardiovascular Center Research Institute, Osaka, Japan; and* [3]*Department of Physical Therapy, Morinomiya University of Medical Sciences, Osaka, Japan*

Submitted 23 November 2010; accepted in final form 26 January 2011

Mizuno M, Kawada T, Kamiya A, Miyamoto T, Shimizu S, Shishido T, Smith SA, Sugimachi M. Exercise training augments the dynamic heart rate response to vagal but not sympathetic stimulation in rats. *Am J Physiol Regul Integr Comp Physiol* 300: R969–R977, 2011. First published January 26, 2011; doi:10.1152/ajpregu.00768.2010.—We examined the transfer function of autonomic heart rate (HR) control in anesthetized sedentary and exercise-trained (16 wk, treadmill for 1 h, 5 times/wk at 15 m/min and 15-degree grade) rats for comparison to HR variability assessed in the conscious resting state. The transfer function from sympathetic stimulation to HR response was similar between groups (gain, 4.2 ± 1.5 vs. 4.5 ± 1.5 beats·min^{-1}·Hz^{-1}; natural frequency, 0.07 ± 0.01 vs. 0.08 ± 0.01 Hz; damping coefficient, 1.96 ± 0.55 vs. 1.69 ± 0.15; and lag time, 0.7 ± 0.1 vs. 0.6 ± 0.1 s; sedentary vs. exercise trained, respectively, means ± SD). The transfer gain from vagal stimulation to HR response was 6.1 ± 3.0 in the sedentary and 9.7 ± 5.1 beats·min^{-1}·Hz^{-1} in the exercise-trained group ($P = 0.06$). The corner frequency (0.11 ± 0.05 vs. 0.17 ± 0.09 Hz) and lag time (0.1 ± 0.1 vs. 0.2 ± 0.1 s) did not differ between groups. When the sympathetic transfer gain was averaged for very-low-frequency and low-frequency bands, no significant group effect was observed. In contrast, when the vagal transfer gain was averaged for very-low-frequency, low-frequency, and high-frequency bands, exercise training produced a significant group effect ($P < 0.05$ by two-way, repeated-measures ANOVA). These findings suggest that, in the frequency domain, exercise training augments the dynamic HR response to vagal stimulation but not sympathetic stimulation, regardless of the frequency bands.

heart rate variability; transfer function; systems analysis

HEART RATE VARIABILITY (HRV) is considered to be a useful noninvasive assessment of autonomic nervous system activity. It has been well recognized that exercise training increases HRV at rest (4, 19). A recent meta-analysis by Sandercock et al. (28) demonstrated that exercise training results in significant increases in R-R interval and high-frequency (HF) power of HRV. Nevertheless, not all studies have demonstrated increases in HRV after exercise training (7). To date, the exact mechanisms underlying increases in HRV after exercise training remain to be elucidated. Many earlier studies have suggested that the augmentation of HRV induced by exercise training may be caused by a withdrawal of sympathetic tonus and/or an increase in vagal tonus (5, 14, 36). Autonomic tone assessed by HRV may reflect both the autonomic outflow from the central nervous system and the peripheral autonomic regulation of atrial pacemaker cells. The latter can be assessed quantitatively by examining the heart rate (HR) response to electrical stimulation of the autonomic nerves. Furthermore, recent studies suggested that peripheral autonomic regulation of atrial pacemaker cells could contribute to the exercise training-induced increases in cardiac vagal function (9, 10).

Equivocal results, however, have been reported using autonomic nerve stimulation. Regarding the vagal system, the effects of exercise training have been inconsistent among studies, showing both increases (9, 10) and reductions in vagally stimulated HR control (25). When considering the sympathetic system, a previous study demonstrated that the HR response to sympathetic stimulation was reduced by exercise training (22). However, the mechanisms underlying the training effect are controversial (3, 15, 26, 29, 33, 35). These equivocal results could be explained by differences in species and modes of exercise training among studies (i.e., exercise type, intensity, and duration, etc.). More importantly, since these studies of autonomic nerve stimulation did not evaluate HRV, a causal relationship between increased HRV and adaptation in peripheral autonomic HR control remains largely undetermined. Furthermore, despite the fact that HRV has been evaluated by using frequency domain as well as time domain analyses, to date, there are no reports available examining the effects of exercise training on the dynamic HR response to sympathetic or vagal stimulation in the frequency domain. Analysis of peripheral autonomic regulation in the frequency domain would advance our understanding of the mechanisms responsible for the alterations in HRV that occur in response to exercise training.

We have recently developed a technique to assess the dynamic characteristics of HR control by the autonomic nervous system in rats using transfer function analysis (21). The transfer function analysis can quantitatively evaluate the HR response to autonomic nerve stimulation over a wide frequency range that is necessary for interpreting the generation of HRV. Therefore, the aims of the present study were *1*) to identify the dynamic characteristics of sympathetic and vagal HR control in exercised-trained rats and *2*) to determine whether alterations in peripheral autonomic regulation contribute to changes in the frequency components of HRV in exercised-trained rats.

MATERIALS AND METHODS

Animal Care and Training Program

Animal care was in accordance with the "Guiding Principles for Care and Use of Animals in the Field of Physiological Sciences," approved by the Physiological Society of Japan. All protocols were reviewed and approved by the Animal Subjects Committee of the

Address for reprint requests and other correspondence: M. Mizuno, Dept. of Physical Therapy, Univ. of Texas Southwestern Medical Center at Dallas, 5323 Harry Hines Blvd., Dallas, TX 75390-9174 (e-mail: masaki.mizuno@utsouthwestern.edu).

National Cerebral and Cardiovascular Center. Fourteen male Sprague-Dawley rats (200–250 g body wt) were fed standard laboratory chow and water ad libitum and housed three per cage in a temperature-controlled room with a 12:12-h dark-light cycle. Rats were randomly assigned to one of two groups: sedentary ($n = 7$) and exercise trained ($n = 7$).

Exercise training was performed on a motor-driven treadmill, 5 days/wk for 16 wk, gradually progressing toward a speed of 15 m/min at a 15-degree grade for 60 min. Sedentary rats walked (10 m/min at 15 degrees) 10 min/day once per week during the 16-wk period to maintain treadmill familiarity. At the end of the 16-wk period, maximal exercise capacity was measured twice in each rat in tests separated by 2 days (6). The protocol for the maximal exercise capacity test consisted of walking at 10 m/min for 5 min followed by 2 m/min increases in speed every 2 min until the rat reached exhaustion. Rats were considered exhausted when they failed to stay off of a shock bar.

Assessment of Autonomic Tone in the Conscious Resting State

After the performance test, three steel electrodes were implanted under anesthesia. These electrodes were utilized for monitoring the electrocardiogram. The R-R interval was measured using a cardiotachometer (model AT601G; Nihon Kohden, Tokyo, Japan). On the first day of the study, which was 24 h after electrodes had been implanted, resting HR was recorded to analyze the R-R interval variability in the quiet unrestrained rat that was kept in a small box. In accordance with a previous study (25), autonomic tone was assessed by intraperitoneal injections of methylatropine (3 mg/kg) and propranolol (4 mg/kg). Immediately after resting HR was recorded, methylatropine was injected. Since the HR response to methylatropine reached its peak in 10–15 min, this time interval was allocated before the HR measurement. Propranolol was injected after methylatropine injection, and again the HR was measured after 10–15 min. Intrinsic HR was evaluated after simultaneous blockade by propranolol and methylatropine. Sympathetic tonus was defined as the difference between the HR after methylatropine injection and intrinsic HR. On the second day, propranolol was administered first to obtain the inverse sequence of blockade. Vagal tonus was defined as the difference between the HR after propranolol injection and intrinsic HR.

Sympathetic and Vagal Stimulation

Surgical preparations. After obtaining data for the assessment of autonomic tone and HRV, rats were anesthetized by a mixture of urethane (250 mg/ml) and α-chloralose (40 mg/ml), initiated with an intraperitoneal bolus injection of 1 ml/kg. If additional anesthesia was needed, 0.1 ml/kg was given intraperitoneally. The rats were intubated and mechanically ventilated with oxygen-enriched room air. The rats were slightly hyperventilated to suppress chemoreflexes. A catheter was placed in the right femoral artery and connected to a pressure transducer (model DX-200; Nihon Kohden, Tokyo, Japan) to measure arterial pressure (AP). HR was measured using a cardiotachometer (model AT601G; Nihon Kohden) triggered by the R wave on the electrocardiogram. A catheter was introduced into the right femoral vein for drug administration. Sinoaortic barodenervation was performed bilaterally to minimize changes in sympathetic efferent nerve activity via arterial baroreflexes. The vagi were sectioned bilaterally at the neck. A pair of bipolar stainless steel electrodes was attached to the right cervical sympathetic nerve for efferent sympathetic stimulation or the right cervical vagus for efferent vagal stimulation. The stimulation electrodes and nerve were secured with silicon glue (Kwik-Sil; World Precision Instruments, Sarasota, FL). Body temperature was monitored with a thermometer placed in the rectum and was maintained at 38°C with a heating pad throughout the experiment.

Experimental procedures. The pulse duration was set at 2 ms and the stimulation amplitude was fixed at 10 V for both sympathetic and vagal nerve stimulation. To allow for stabilization of hemodynamics, sympathetic and vagal nerve stimulations were started ~1 h after the end of surgical preparations. Between sympathetic and vagal stimulation protocols > 15 min elapsed to allow AP and HR to return to their respective baseline values.

To estimate the dynamic transfer characteristics from sympathetic stimulation to HR response, the sectioned end of the right cervical sympathetic nerve was stimulated employing a frequency-modulated pulse train for 10 min. The stimulation frequency was switched every 1,000 ms to either 0 or 5 Hz according to a binary white noise signal. The power spectrum of the stimulation signal was reasonably constant up to 0.5 Hz. The transfer function was estimated up to 0.5 Hz because the reliability of estimation decreased due to the diminution of input power above this frequency. The selected frequency range sufficiently spanned the range of physiological interest (21). For estimation of the static transfer characteristics from sympathetic stimulation to HR response, stepwise sympathetic stimulation was performed. Sympathetic stimulation frequency was increased from 1 to 5 Hz in 1-Hz increments. Each frequency step was maintained for 60 s.

To estimate the dynamic transfer characteristics from vagal stimulation to HR response, the right vagus was stimulated employing a frequency-modulated pulse train for 10 min. The stimulation frequency was switched every 500 ms to either 0 or 10 Hz according to a binary white noise signal. The power spectrum of the stimulation signal was reasonably constant up to 1 Hz. The transfer function was estimated up to 1 Hz because the reliability of estimation decreased due to the diminution of input power above this frequency. The selected frequency range sufficiently spanned the range of physiological interest (21). For estimation of the static transfer characteristics from vagal stimulation to HR response, stepwise vagal stimulation was performed. Vagal stimulation frequency was changed among 2, 4, 8, 16, and 32 Hz. Each frequency step was maintained for 60 s.

Data Analysis

Spectral analysis of HRV. Data obtained during the conscious resting state were digitized at 200 Hz utilizing a 12-bit analog-to-digital converter and stored on the hard disk of a dedicated laboratory computer system. Beat-by-beat time series of the R-R interval were interpolated every 130 ms (Δt). Twelve data segments of 512 (N) points overlapping half of the preceding data were processed. For each data segment, after the linear trend was removed and the Hanning window applied, power spectral density was computed using the fast Fourier transform algorithm. The frequency resolution was $\Delta f = 1/(N \Delta t)$, i.e., 0.015 Hz, and the highest frequency was $\Delta f = 1/2\Delta t$, i.e., 3.85 Hz, where f is frequency. The very-low-frequency (VLF) band ranged between 0.017 and 0.27 Hz, the low-frequency (LF) band between 0.27 and 0.75 Hz, and the high-frequency (HF) band between 0.75 and 3.3 Hz, according to an earlier report (8). The percentage of LF or HF power relative to the sum of LF and HF powers and the ratio of LF to HF power were also calculated.

Transfer function analysis. The dynamic characteristics of the HR response to sympathetic or vagal stimulation were estimated by a transfer function analysis (see APPENDIX for details). Dynamic sympathetic control of HR was quantified by fitting a second-order low-pass filter with pure delay to the estimated transfer function. The dynamic vagal control of HR was quantified by fitting a first-order, low-pass filter with pure delay to the estimated transfer function. To facilitate the intuitive understanding of the system's dynamic characteristics, we calculated the system step response of HR to 1-Hz nerve stimulation as follows.

The system impulse response was derived from the inverse Fourier transform of the transfer function. The system step response was then obtained from the time integral of the impulse response. The length of the step response was 51.2 s. The 80% rise time for the sympathetic step response or the 80% fall time for the vagal step response was estimated as the time at which the step response reached 80% of the

Table 1. *Physical characteristics*

	Sedentary	Exercise Trained
Body weight, g	642 ± 33	534 ± 33*
Ventricular weight, g	1.22 ± 0.03	1.17 ± 0.04*
Ventricular weight/body weight, g/kg	1.9 ± 0.1	2.2 ± 0.1*
Lung weight, g	2.13 ± 0.27	1.89 ± 0.38
Lung weight/body weight, g/kg	3.3 ± 0.3	3.5 ± 0.7
Performance test, s	1150 ± 165	1790 ± 389*

Values are means ± SD. *$P < 0.05$ compared with sedentary group.

steady-state response calculated by averaging the last 10 s of data of the step response.

Statistical Analysis

All data are represented as means ± SD. Data were analyzed using unpaired Student's *t*-tests (sedentary vs. exercise trained) or two-way, repeated-measures ANOVA. Values of $P < 0.05$ were considered to be significant.

RESULTS

Physical Characteristic

Morphometric characteristics and exercise capacity for sedentary and exercised-trained rats are presented in Table 1. The mean body weight of the exercised-trained rats was significantly smaller than that of the sedentary rats. The mean ventricular weight of the exercised-trained rats was slightly but significantly smaller than that of the sedentary rats. Consequently, the ventricular weight normalized by body weight was significantly greater in the exercised-trained compared with the sedentary group. The lung weight-to-body weight ratio was not different between the groups. Exercise capacity was 64% greater in the exercised-trained than in the sedentary group. The reproducibility of measuring the maximal exercise capacity was reasonably high ($y = 1.2x - 226.1$, $R^2 = 0.79$; x and y represent the first and second measurements).

Spectral Analysis of HRV and Autonomic Tone in the Conscious Resting State

The power spectral densities of R-R interval are shown in Table 2. The percentage of LF power was significantly smaller, and the percentage of HF power was significantly greater in the exercised-trained rats than in the sedentary rats. The LF/HF ratio in the exercised-trained rats was significantly smaller compared with that in the sedentary rats. HR at rest was significantly lower in the exercised-trained compared with the sedentary group (Fig. 1*A*). The intrinsic HR was similar between the groups (Fig. 1*A*). Although the sympathetic tonus was comparable between the groups, the vagal tonus tended to be greater ($P = 0.08$) in the exercised-trained compared with the sedentary group (Fig. 1*B*).

Dynamic Sympathetic and Vagal Transfer Functions

Table 3 summarizes hemodynamics during dynamic sympathetic stimulation. Sympathetic stimulation significantly increased mean HR in both sedentary and exercised-trained groups. Mean HR and AP did not differ between the groups, before and during sympathetic stimulation. Figure 2*A* illustrates the dynamic transfer function characterizing sympathetic HR control. The frequency band effect was significant ($P < 0.0001$) but the group effect was insignificant ($P = 0.5461$) in the dynamic gain values of the sympathetic transfer function by two-way, repeated-measures ANOVA. The parameters of the sympathetic transfer function were comparable between the groups (Table 4). Figure 2*B* shows the calculated step response of HR to sympathetic stimulation. The steady-state response and the 80% rise time did not differ significantly between the groups (Table 4).

Table 5 summarizes hemodynamics during dynamic vagal stimulation. Vagal stimulation significantly decreased mean HR in both sedentary and exercised-trained groups. Mean HR and AP did not differ between the groups, before and during vagal stimulation. Figure 3*A* illustrates the dynamic transfer function characterizing vagal HR control. The frequency band effect ($P < 0.0001$) and the group effect ($P < 0.0001$) were both significant in the dynamic gain values of the vagal transfer function by two-way, repeated-measures ANOVA. The estimated dynamic gain (*see* APPENDIX) tended to be greater in the exercised-trained compared with the sedentary group ($P = 0.06$, Table 6). Other parameters did not differ between the groups. Figure 3*B* shows the calculated step response of HR to vagal stimulation. The calculated steady-state response in the exercised-trained rats also tended to be greater than that in the sedentary rats ($P = 0.06$, Table 6). There was no significant difference in the 80% fall time between the groups.

Dynamic Gain Values of Sympathetic and Vagal Transfer Function Corresponding to HRV Frequency Bands

When dynamic gain values of the sympathetic transfer function were averaged for the VLF and LF (up to 0.5 Hz, see METHODS) bands, the frequency band effect was significant, but the group effect was insignificant by two-way, repeated-measures ANOVA (Fig. 4*A*). When dynamic gain values of the vagal transfer function were averaged for the VLF, LF, and HF (up to 1 Hz, see METHODS) bands, the frequency band effect was insignificant but the group effect was significant such that the dynamic gain was significantly greater in the exercised-trained compared with the sedentary group (Fig. 4*B*).

Static Sympathetic and Vagal Transfer Function

The increase in HR with stepwise sympathetic stimulation was similar between groups (Fig. 5*A*). The stimulation frequency effect was significant, while the group effect was insignificant by two-way, repeated-measures ANOVA. In contrast, the decrease in HR with stepwise vagal stimulation was greater in the exercised-trained compared with sedentary rats (Fig. 5*B*). Both the stimulation frequency effect and the group effect were significant.

Table 2. *Spectral parameters of R-R interval*

	Sedentary	Exercise Trained
Variance, ms^2	87 ± 39	90 ± 32
VLF, ms^2	73 ± 30	80 ± 30
LF, ms^2	6.3 ± 3.4	3.1 ± 3.0
LF, %	49 ± 11	36 ± 7*
HF, ms^2	8.0 ± 7.6	6.2 ± 7.1
HF, %	51 ± 11	64 ± 7*
LF/HF ratio	1.0 ± 0.5	0.6 ± 0.2*

Values are means ± SD. LF, low frequency; VLF, very low frequency; HF, high frequency; *$P < 0.05$ compared with sedentary group.

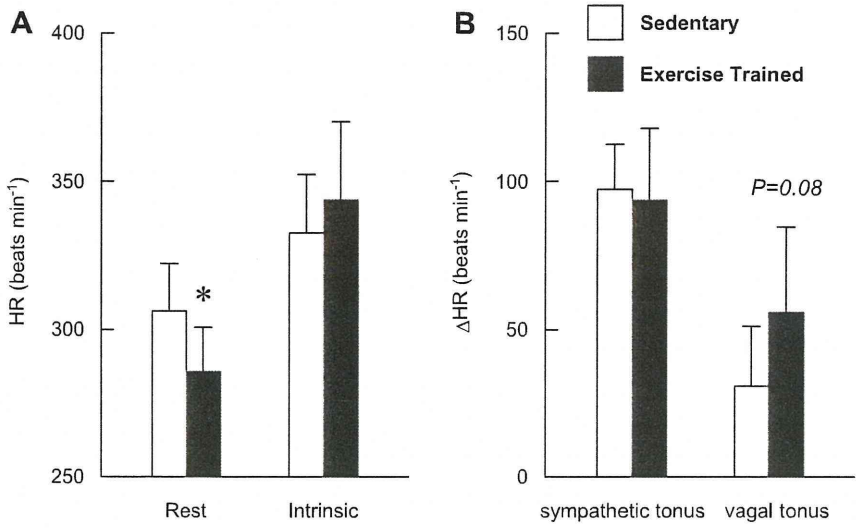

Fig. 1. Heart rate (HR) at rest and intrinsic HR (*A*) and HR sympathetic and vagal tone (*B*) obtained in sedentary and exercised-trained rats. *$P < 0.05$ compared with sedentary group.

DISCUSSION

We have examined the dynamic transfer function of autonomic HR control by using random binary sympathetic and vagal nerve stimulation in sedentary and exercised-trained rats. The major findings in the present study are *1*) that the exercise training did not alter the sympathetic transfer function substantially but augmented the dynamic gain of the vagal transfer function; and *2*) in the frequency domain, exercise training increased the dynamic HR response to vagal stimulation but not sympathetic stimulation, regardless of the frequency band. These findings are the first quantitative data on the effect of exercise training on the dynamic characteristics of peripheral HR control by the sympathetic and vagal systems.

Validity of Exercise Training

The relative ventricular hypertrophy and higher exercise capacity in the exercised-trained compared with the sedentary group suggested that exercise program used in the present study was sufficient to induce physiological adaptations commensurate with an effective training stimulus. As is well known, exercise training induces bradycardia at rest (Fig. 1*A*). Moreover, changes in the spectral parameters for R-R interval (Table 2) and autonomic tone (Fig. 1*B*) induced by the exercise training are consistent with earlier studies in rats (30, 31).

Effect of Exercise Training on Sympathetic and Vagal Transfer Function

Exercise training altered neither dynamic (Fig. 2) nor static sympathetic transfer function (Fig. 5*A*). These results are different than those reported in a previous study in which swim training significantly reduced the HR response to sympathetic nerve stimulation in a double atrial/right stellate ganglion preparation in guinea pigs (22). The discrepancy between investigations may have arisen from differences in the nerves experimentally stimulated (cervical sympathetic nerve vs. stellate ganglion), animal species studied (rats vs. guinea pigs), and/or experimental preparation utilized (in vivo vs. ex vivo). The mechanisms underlying the sympathetically mediated exercise training effect on HR are also controversial. For instance, chronotropic responsiveness to isoproterenol has been reported to be decreased in one study (15) but unchanged in another (22) by exercise training. Furthermore, in response to exercise training, the density and affinity of β-adrenoceptors in the heart have been shown to be reduced in some reports (26, 33), while unchanged in others (3, 34, 35).

Table 3. *Arterial pressure(AP) and heart rate (HR) during dynamic sympathetic stimulation protocol*

	Sedentary		Exercise Trained	
	Prestimulation	During Stimulation	Prestimulation	During Stimulation
AP. mmHg	74 ± 16	68 ± 15†	89 ± 17	84 ± 24
HR. beats/min	377 ± 25	444 ± 23†	381 ± 16	444 ± 26†

Values are means ± SD. †$P < 0.05$ compared with prestimulation.

Exercise training augmented the dynamic gain of the vagal transfer function (Fig. 2). The effect of exercise training was also significant for static vagal transfer function (Fig. 5*B*). These results are in agreement with previous studies showing that exercise training significantly augmented the HR response to vagal nerve stimulation in a double atrial/right vagal nerve preparation using mice (9, 10). In contrast, Negrao et al. (25) demonstrated that the HR response to vagal stimulation was depressed in exercised-trained rats. A possible explanation for this disparate result is that the arterial baroreflexes remained intact in the experimental preparation used in the study (25). In contrast, sinoaortic barodenervation was performed in the present investigation to minimize baroreflex-mediated changes in sympathetic efferent nerve activity. Exercise training has been shown to attenuate the baroreflex-mediated sympathetic nerve response to hypotension (11). Although speculative, in the study by Negrao et al. (25), baroreflex-mediated sympathetic activation in response to vagally-induced hypotension might have been less in exercised-trained compared with sedentary rats. Consequently, the gain of vagal stimulation might have been attenuated in exercised-trained animals relative to sedentary rats. This suggestion is reasonable given that accentuated antagonism is indicative of a diminution in background sym-